RECIPROCALLY INHIBITORY CIRCUITS OPERATING WITH DISTINCT MECHANISMS ARE DIFFERENTLY ROBUST TO PERTURBATION AND MODULATION

Ekaterina O. Morozova morozova.e.o@gmail.com https://orcid.org/0000-0001-9131-7756
Peter Newstein pnewstein@uoregon.edu https://orcid.org/0000-0003-2966-783X
Eve Marder marder@brandeis.edu http://orcid.org/0000-0001-9632-5448

Volen Center and Department of Biology, Brandeis University, Waltham, MA, USA 02453

Running title: Robustness of reciprocally inhibitory circuits

Highlights

- The synaptic threshold determines the mode of reciprocal inhibitory circuits.
- Robust oscillatory escape mode circuits rely on tight conductance correlations.
- Release mode circuits are sensitive to temperature and neuromodulation.
- Mixed mode circuits are sensitive to neuronal excitability differences.

Summary

What features are important for circuit robustness? Reciprocal inhibition is a building block in many circuits. We used dynamic clamp to create reciprocally inhibitory circuits from GM neurons of the crab stomatogastric ganglion by injecting artificial synaptic and hyperpolarization-activated inward (H) currents. In “release”, the active neuron controls the off/on transitions. In “escape”, the inhibited neuron controls the transitions. We characterized the robustness of escape and release circuits to alterations in circuit parameters, temperature, and neuromodulation. Escape circuits rely on tight correlations between synaptic and H conductances to generate bursting but are resilient to temperature increase. Release circuits are robust to variations in synaptic and H conductances but fragile to temperature increase. The modulatory current (I_{MI}) restores oscillations in release circuits but has little effect in escape. Thus, the same perturbation can have dramatically different effects depending on the circuits’ mechanism of operation that may not be observable from circuit output.

keywords: half-center oscillator; mutual inhibition; oscillations; dynamic clamp; release; escape; temperature; I_{MI}

Introduction

Neuronal circuits show a high level of degeneracy in their intrinsic and synaptic properties, with multiple conductances with overlapping voltage and time dependence (Goaillard and Marder, 2021). Previous studies demonstrated that neuronal networks with similar underlying parameters that generate similar behavior can respond differently to perturbations (Alonso and Marder, 2020; Prinz et al., 2004; Tang et al., 2012). Reciprocal inhibition is ubiquitous in nervous systems, where it has many functions. Lateral inhibition is important in many sensory systems, and reciprocal inhibition between individual neurons or groups of neurons is the "building block" of many half-center oscillators that generate antiphase and multiphase activity patterns (Arbas and Calabrese, 1987a, b; Brown, 1911; Calabrese, 1998; Getting, 1989; Marder and Calabrese, 1996; Perkel and Mulloney, 1974; Sakurai and Katz, 2016; Satterlie, 1985; Soffe et al., 2001; Zang et al., 2020). Due to their well-defined output, small reciprocally inhibitory circuits provide an excellent platform for investigating the resilience of circuits to internal and environmental challenges.

Theoretical studies have described two fundamentally different mechanisms of antiphase oscillations in half-center circuits: "release" and "escape" (Skinner et al., 1994; Wang and Rinzel, 1992). In the release mode the presynaptic cell falls below its synaptic threshold, thus, releasing the inhibited cell. In escape, the inhibited cell depolarizes above its synaptic threshold, thus, terminating the firing of the active cell. Whether the oscillator exhibits the escape or release mechanism depends on the position of the synaptic threshold within the slow-wave envelope of the membrane potential oscillation (Skinner et al., 1994; Wang and Rinzel, 1992). Many factors affect neuronal membrane potential and the synaptic threshold, including neuromodulators, temperature, and changes in the composition of the extracellular fluid.

Some of the theoretical predictions of how oscillations are generated and controlled in reciprocally inhibitory circuits were tested in biological neurons by Sharp et al. (1996) and Grashow et al (2009). They used the dynamic clamp, which utilizes a real-time computer interface to simulate nonlinear voltage-dependent synaptic and intrinsic currents in biological cells. Sharp et al. (1996) studied the effects of varying computer-generated parameters on the circuit output and confirmed theoretical

predictions that the switch in the mechanism of oscillations in a biological network is possible by shifting the synaptic threshold. Grashow et al. (2009) extended their work by studying the effects of the neuromodulators, oxotremorine and serotonin, on the dynamic clamp created half-center networks. They observed a substantial variability in individual circuit responses to neuromodulation.

Most theoretical studies on half-center oscillators were done with two identical neurons (Daun et al., 2009; Nadim et al., 1995; Skinner et al., 1994; Wang and Rinzel, 1992; Zhang and Lewis, 2013) with the notable exception of Onasch and Gjorgieva (2020). In some biological systems, half-center oscillators are formed between pairs of neurons that are ostensibly “identical” or are copies of the same neuron type, such as, in the leech heartbeat system or sea slugs escape swimming central-pattern generators (CPGs) (Katz, 2016; Marder and Calabrese, 1996; Sakurai and Katz, 2016). That said, even when biological half-center oscillators are formed from the reciprocal inhibition of two neurons of the same cell type, there is always some variability between those neurons. Reciprocal inhibition between different classes of neurons can also be crucial for the operation of central pattern generating or other circuits, such as in the stomatogastric ganglion (Bartos et al., 1999; Blitz and Nusbaum, 2011; Marder and Bucher, 2007; Marder and Calabrese, 1996). In this case, there is no presumption that the intrinsic properties of the two neurons are identical. In this paper we exploit the biological variability between the neurons we study to examine the robustness of the half-center oscillator on the extent of asymmetry between the two neurons used to form the half-center.

Although it is known that half-center oscillators can operate with a mixed mechanism (Angstadt and Calabrese, 1989, 1991; Calabrese et al., 2016; Hill et al., 2001), these have been less studied than oscillators in the pure release or pure escape mechanisms. Here, we also look at the increased or decreased resilience of oscillators operating in a mixed regime, as modulation and other perturbations often lead to half-centers operating in a mixture of mechanisms.

We performed dynamic clamp experiments of half-center oscillators using temperature and neuromodulation as perturbations to address some of the following questions. Are circuits with different underlying mechanisms of oscillation equally robust

to intrinsic and environmental perturbations? What are the factors that play a key role in immediate circuit resilience against perturbations? What role does the dynamical mechanism of oscillation play in the circuit responses to neuromodulation? How does asymmetry between the units forming a half-center oscillator affect the output of the circuit?

Results

The output of reciprocally inhibitory neurons is shaped by their intrinsic and synaptic properties

To explore the interactions between intrinsic and synaptic parameters underlying variability in circuit behaviors and differential robustness to perturbations, we used the dynamic clamp to build half-center oscillator circuits using pharmacologically isolated gastric mill (GM) neurons of the stomatogastric ganglion (STG) of the crab *Cancer borealis* (Figure 1A, STAR Methods). Half-center circuits were formed by connecting two neurons via artificial reciprocal inhibitory synapses and by adding hyperpolarization-activated inward (H) currents, following the methods described in Sharp et al. (1996). Activation curves for the synaptic and H currents are shown in Figure 1B.

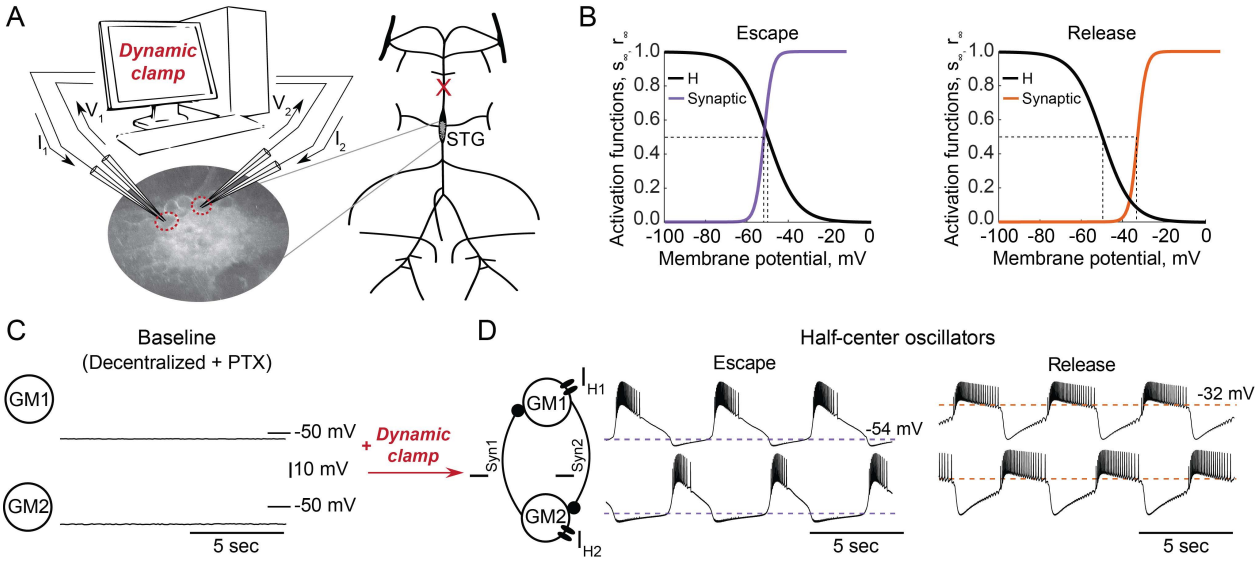

Figure 1. Experimental set-up. A) Half-center oscillator circuits are built by connecting two gastric mill (GM) neurons from the stomatogastric ganglion (STG) of the crab *Cancer borealis* via artificial reciprocal inhibitory synapses (I_{Syn}) and by adding an artificial hyperpolarization-activated inward current (I_H) in two-electrode dynamic-clamp mode using RTXI. **B)** Activation curves of the dynamic clamp generated H current and synaptic current. Shift in the synaptic activation curve switches the mechanism of oscillations between escape (left graph, purple curve) and release (right graph, orange curve). **C)** At baseline, synaptically isolated GM neurons are silent with a resting membrane potential between -65 and -55 mV. **D)** When coupled via the dynamic clamp, neurons generate alternating bursting pattern of activity (half-center oscillator). Representative half-center oscillator traces with escape mechanism are shown on the left and with release mechanism on the right. Synaptic thresholds are indicated by the horizontal dashed lines. In the circuit diagram, filled circles indicate inhibitory synapses.

GM neurons are silent in the absence of modulatory and synaptic inputs (Figure 1C) and fire tonically when depolarized. When coupled together via reciprocal inhibitory connections they can generate an antiphase bursting patterns of activity (Figure 1D). There are two fundamental mechanisms of antiphase bursting in these circuits – "release" and "escape" (Wang and Rinzel, 1992; (Skinner et al., 1994). The mechanism of oscillation depends on the position of the synaptic threshold within the slow-wave envelope of the membrane potential oscillations. Low thresholds that are close to the most hyperpolarized portion of the slow-wave generate an escape mechanism, while high synaptic thresholds that are close to the top of the slow-wave envelope lead to a release mechanism (Figure 1D). By shifting the synaptic activation curve via dynamic clamp, we change the mechanism of oscillation (Figure 1B).

Characteristics of half-center oscillator output depend on the mechanism of oscillation

We investigated the dependence of the output of half-center oscillator circuits on the synaptic threshold while fixing the synaptic and H conductances. In each experiment we varied the synaptic threshold from -54 to -28 mV in 2 mV steps (N=16, Figure 2A). We then characterized how physiologically relevant properties of the circuit output, e.g., the cycle frequency, amplitude of oscillations, duty cycle, spike frequency and number of spikes per burst depend on the synaptic threshold (Figure 2B). Because of the inherent intrinsic differences in the biological neurons that comprise the half-centers, the same value of synaptic threshold does not necessarily generate the same mechanism of oscillation across preparations, as the relative position of the threshold within the slow-wave and the excitability of the neurons define the mechanism of oscillation. Thus, to quantitatively characterize the mechanism of oscillation across preparations, we introduce a measure of the mechanism of oscillation called Escape to Release Quotient (ERQ). This allowed us to characterize the mechanism of oscillation in response to perturbations or changes in circuit parameters. We defined ERQ with the following equation:

$$ERQ = \frac{\overline{V_M} - V_{th}}{\overline{V_M}}.$$

$\overline{V_M}$ is a mean membrane potential averaged across both neurons in a circuit and V_{th} is a synaptic threshold.

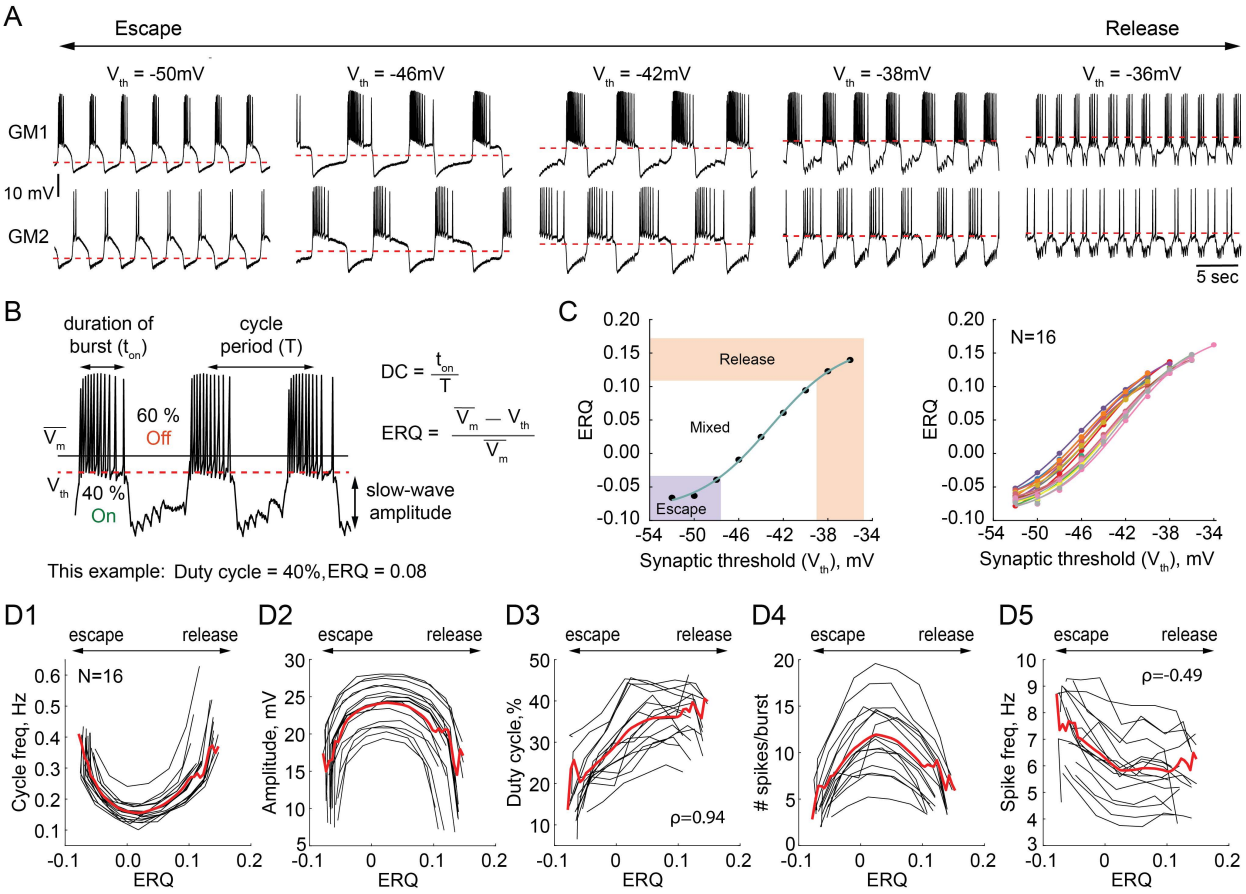

Figure 2. Dependence of the characteristics of half-center oscillator output on the mechanism of oscillation. **A)** Representative intracellular recordings of GM neurons coupled via the dynamic clamp to form a half-center oscillator for different synaptic thresholds (V_{th}). Depolarization of the synaptic threshold switches the mechanism of oscillations from escape to release passing through a mixture of mechanisms. **B)** Half-center oscillator activity characteristics measured in this study, such as cycle period (frequency), slow-wave amplitude and duty cycle (DC) are indicated on the example GM neuron trace. Escape to Release Quotient (ERQ) is calculated based on the mean membrane potential and the synaptic threshold as shown. **C)** ERQ as a function of the synaptic threshold for a single preparation (left) and multiple preparations (N=16, right). Relationship between the ERQ and the synaptic threshold is sigmoidal as shown by the fit curve (cyan). Left hand ERQ plot is from the experiment shown in (A) **D1)** Cycle frequency vs ERQ. **D2)** Slow-wave amplitude vs ERQ. **D3)** Duty cycle vs ERQ. **D4)** Number of spikes per burst vs ERQ. **D5)** Spike frequency vs ERQ. Black lines are individual experiments (N=16), red lines represent means across all the experiments.

The left panel of Figure 2C shows that the relationship between the synaptic threshold and ERQ is well fit by a sigmoidal function ($R^2 = 0.998$). At the top of the sigmoid (above 0.11 in Figure 2C) the circuits are in a release mechanism. At the

bottom of the sigmoid (below -0.033 in Figure 2C) the circuits are in an escape mechanism. The threshold ERQ values for release and escape were defined based on the maximum and minimum of the second derivative of the sigmoid functions that were fit to ERQ vs V_{th} data for each experiment. The ERQ threshold for escape is -0.038 ± 0.008, while the ERQ threshold for release is 0.105 ± 0.012. The near-linear portion of the sigmoidal curve corresponds to a mixture of the mechanisms. The mixed regime demonstrates characteristics of both mechanisms with various balances between the mechanisms depending on the relative position of the threshold within the slow-wave envelope. The right panel in Figure 2C shows the dependence of the ERQ on the synaptic threshold across 16 preparations.

The cycle frequency shows a U-shaped relation as a function of the ERQ (Figure 2D1), as also seen in Sharp et al (1996). The slow-wave amplitude shows an inverted U-shaped dependence on the ERQ and is inversely correlated with the cycle frequency (Figure 2D2, Pearson correlation coefficient $r = -0.9$). The duty cycle (the burst duration divided by the cycle period) increases as the mechanism of oscillations changes from escape to release (Figure 2D3, $\rho = 0.94, p < 0.001,$ Spearman rank correlation test). The difference in the duty cycle of circuits with different mechanisms can be explained by the difference in the magnitudes of the synaptic current. Because the synaptic threshold in escape is significantly more hyperpolarized relative to the release case, the magnitude of the synaptic current in a postsynaptic cell during its active phase is larger in the escape mechanism than in release, causing a steep hyperpolarization of the membrane potential below the neuron's spike threshold. The number of spikes per burst also shows an inverted U-shaped dependence on ERQ (Figure 2D4). The spike frequency moderately decreases as the mechanism of oscillation changes from escape to release (Figure 2D5, $\rho = -0.49, p = 3.6 \cdot 10^{-4}$, Spearman rank correlation test). The higher spike frequency in escape mode is caused by a strong rebound current.

Circuit output as a function of synaptic and H conductances in escape vs release

We investigated the dependence of the output of reciprocally inhibitory circuits on their synaptic (g_{Syn}) and H (g_H) conductances. In each experiment we varied g_{Syn} and g_H from 150 nS to 1050 nS in steps, mapping combinations of these parameters to

characteristics of the output of the circuits operating with escape or release mechanisms. Figure 3 summarizes pooled data from 20 experiments. Circuits operating in either release or escape produce stable alternating bursting which is distributed differently in the synaptic and H conductance space (Figure 3A). The gray scale in Figure 3A shows the fraction of bursting circuits operating with escape (left panel, N=10) and release (right panel, N=10) mechanisms at each g_H-g_{Syn} parameter set. There are more circuits that generate half-center activity in release than in escape across these parameters. The synaptic and H currents must be tightly correlated to produce robust bursting in escape, but not in release mode. These findings suggest that half-center oscillators with a release mechanism are more robust to changes in either synaptic or H conductances, compared to half-centers with an escape mechanism. In addition, these results provide a potential explanation of the across-preparation variability in conductance sets leading to stable bursting in reciprocally inhibitory circuits with a fixed synaptic threshold observed by Grashow et al. (2009).

Figure 3B-F characterizes the dependence of cycle frequency, oscillation amplitude, duty cycle, spike frequency and the number of spikes per burst on synaptic and H conductances. Increase in H current decreases the cycle frequency of the circuits in release (Figure 3B, right panel), but increases the cycle frequency in escape (Figure 3B, left panel). In escape, increasing the H conductance helps the inhibited neuron depolarize above the synaptic threshold faster, thus increasing the oscillation frequency. In release, increasing the H conductance prolongs the active phase of an uninhibited neuron, thus decreasing the frequency of oscillation. In both cases the oscillation frequency decreases with the increase in inhibitory synaptic conductance (Figure 3B). The slow-wave amplitude (Figure 3C), number of spikes per burst (Figure 3D) and spike frequency (Figure 3E) decrease in the escape circuits but increase in the release circuits when H conductance is increased. The duty cycle is relatively independent of variations in synaptic and H conductances in either release or escape cases (Figure 3F). For all sets of g_{Syn} and g_H, the duty cycles of the escape half-center oscillators are significantly lower than the duty cycles of the release half-center oscillators ($19.5 \pm 3.6\%$ in escape vs $42.4 \pm 3.3\%$ in release, $p < 0.001$, Wilcoxon rank-sum test).

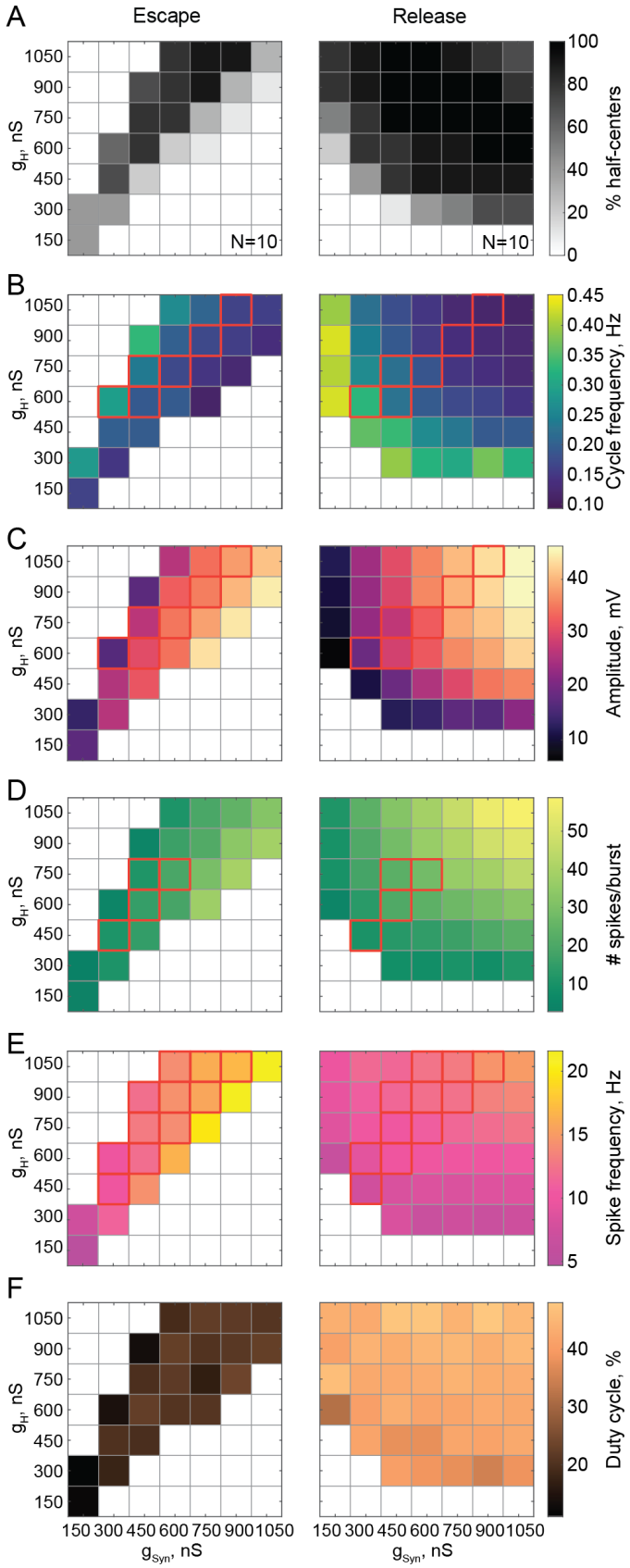

Figure 3. Maps of network output as a function of the synaptic and H conductances (g_{Syn}, g_H) for circuits with escape and release mechanisms. A) Distribution of half-center oscillators in g_{Syn}-g_H parameter space. Gray scale shows the percentage of preparations that formed half-center oscillators for each g_{Syn}-g_H parameter combination withing the map (N=10 for each mechanism). White space corresponds to parameters sets for which no oscillators exist. **B)** Dependence of the mean half-center oscillator cycle frequency on g_{Syn} and g_H across 10 preparations for each mechanism. **C)** Dependence of the mean slow-wave amplitude on g_{Syn} and g_H. **D)** Dependence of the mean number of spikes per burst on g_{Syn} and g_H. **E)** Dependence of the mean spike frequency on g_{Syn} and g_H. **F)** Dependence of the mean duty cycle on g_{Syn} and g_H. In panels B-E, g_{Syn}-g_H parameter sets for which circuit output characteristics were not significantly different between release and escape are indicated by red boxes (Wilcoxon rank-sum test, $p>0.05$).

For a range of g_H-g_{Syn} parameter sets, the characteristics of the output of half-center oscillators with escape and release mechanisms are not statistically different (Figure 3 B-E, indicated by the red boxes, Wilcoxon rank-sum test, $p > 0.05$). Thus, similar circuit function can be produced by both escape and release mechanisms for the same values of synaptic and H conductances, although the duty cycles are more disparate than other measures of circuit performance. Importantly, if the mechanism is not known *a priori*, it is practically impossible to identify it only based on baseline spike output (e.g. in extracellular recordings) without perturbing the system.

Circuits operating in a mixture of mechanisms

In some biological systems, half-center oscillators rely on a mixture of escape and release mechanisms to generate alternating bursting patterns of activity (Angstadt and Calabrese, 1989, 1991; Calabrese et al., 2016; Hill et al., 2001). Neuromodulators can shift the synaptic threshold, thus affecting the mechanism of oscillation in the circuit (Li et al., 2018). We explored how the characteristics of the circuit output mapped onto g_{Syn}-g_H parameter space changed as we transitioned through mechanisms by changing the synaptic threshold. Figure 4 shows the transformation of the g_{Syn}-g_H maps of the network outputs by moving the synaptic threshold from -50 mV to -30 mV in 5 mV steps. The mechanism of oscillation is relatively independent of g_{Syn} and g_H for the extreme cases of the hyperpolarized synaptic thresholds generating an escape mechanism (Figure 4C left panel) and depolarized synaptic thresholds generating a release mechanism (Figure 4C right panel). Nonetheless, the mechanism is sensitive to the changes g_{Syn} and g_H for the intermediate values of the synaptic threshold, as evident by the substantial change in ERQ with g_{Syn} and g_H (Figure 4A, 4C middle panels).

Figure 4A depicts the ERQ and representative half-center voltage traces as a function of g_{syn} and g_H with a synaptic threshold of -40mV. This network is in a mixture of escape and release. The left-hand map illustrates a smooth transition in the mechanism of oscillation as a function of changes in g_{Syn} and g_H. The electrophysiological traces to the right illustrate the activity patterns at different map locations (Figure 4B). Increasing g_H and decreasing g_{Syn} biases the balance towards escape, while decreasing g_H and increasing g_{Syn} biases the mechanism towards

release. Changing the mechanism of oscillation ultimately influences how the circuit will respond to stimuli and perturbations.

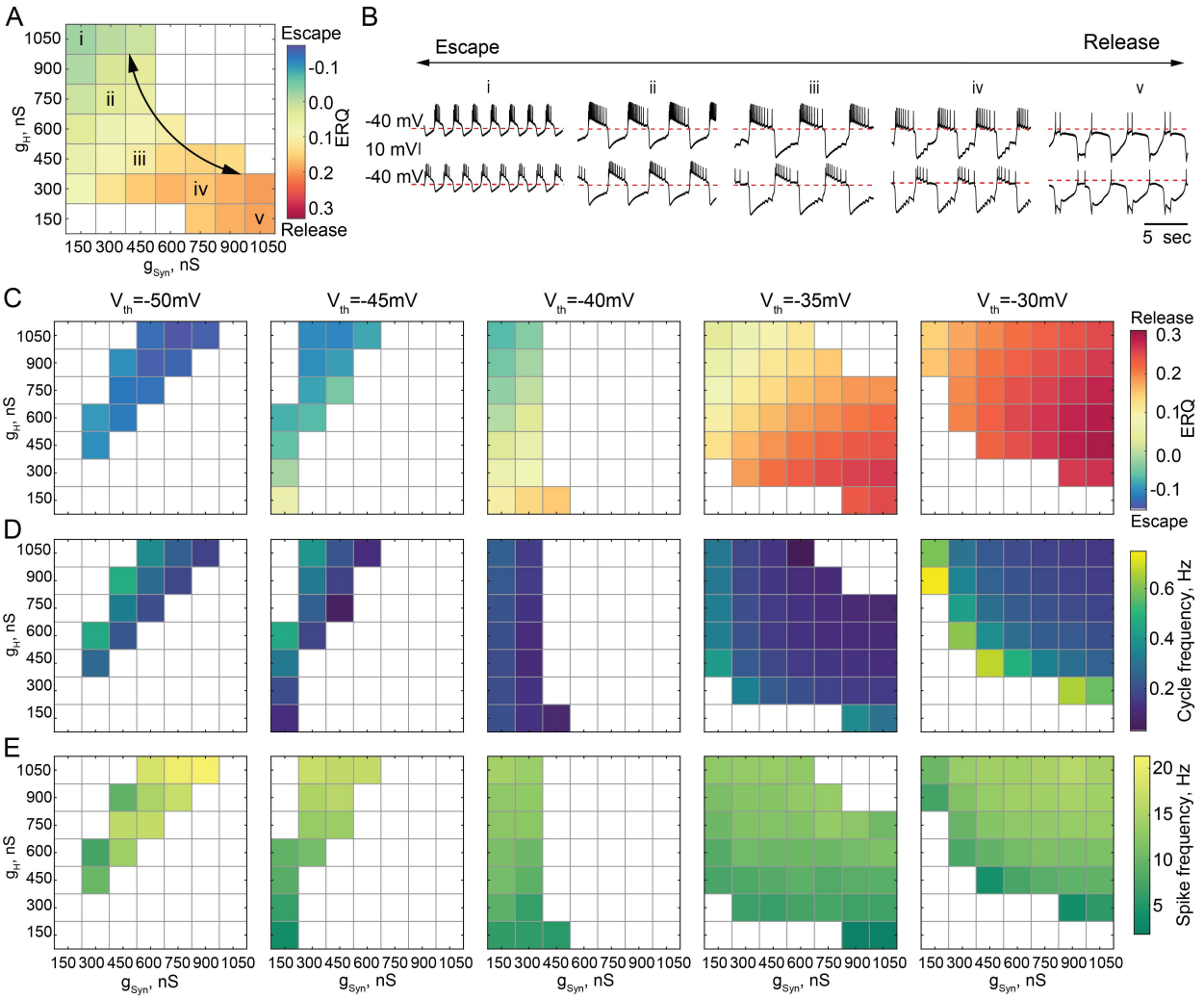

Figure 4. **Dependence of the oscillation mechanism and other half-center activity characteristics on the synaptic and H conductances for different synaptic thresholds.** **A)** ERQ as a function of synaptic and H conductances with a synaptic threshold of -40 mV in a single preparation. Mechanism of oscillations is sensitive to the changes in synaptic and H conductances at V_{th}=-40 mV: an increase in g_{Syn} together with a decrease in g_H switches the mechanism of oscillation from escape (top left corner in the map) to release (bottom right corner in the map). **B)** Representative intracellular recordings of GM neurons coupled via the dynamic clamp corresponding to values of g_{Syn} and g_H indicated in the parameter map (A) by roman numerals. **C)** Dependence of ERQ on g_{Syn} and g_H for the synaptic thresholds of -50 mV, -45 mV, -40 mV, -35 mV and -30 mV in a single preparation. ERQ is relatively insensitive to changes in g_{Syn} and g_H in pure escape (left map) and pure release (right map) cases, but sensitive to g_{Syn} and g_H for intermediate thresholds (middle maps) similar to the experiment shown in panel (A). **D)** Dependence of the half-center oscillator cycle frequency on g_{Syn} and g_H for different synaptic thresholds. **E)** Dependence of the spike frequency on g_{Syn} and g_H for different synaptic thresholds.

Theoretical studies have found that stable bursting is produced when the synaptic threshold is within the slow wave envelope of the membrane potential oscillations (Skinner et al., 1994). Thus, it might appear to be beneficial for the circuit to rely on a mixture of mechanisms, as then the synaptic threshold is far from both the top and bottom of the slow wave. However, we observed that for the intermediate values of the synaptic thresholds (V_{th}=-45, 40 mV, middle maps in Figure 4C), bursting is less regular and exists for a small set of g_{Syn}-g_H on the edge of the map, corresponding to weak synaptic coupling. This is because biological neurons, even of the same type, are never perfectly identical with respect to their intrinsic properties. Thus, the balance between the mechanisms is slightly different in the two cells, leading to situations when one of the cells does not have enough depolarizing drive to escape from inhibition, thus preventing the transition between the states from occurring. Only a small subset of g_{Syn}-g_H parameters allows for a smooth transition from one mechanism to another without losing alternating activity.

We characterized the dependence of cycle frequency, spike frequency, slow-wave amplitude, number of spikes per burst and duty cycle on synaptic and H conductances for different values of synaptic thresholds (Figure 4 and S1). For the synaptic threshold of -40 mV, the cycle frequency is independent of the change in H conductance (Figure 4D middle panel). The spike frequency increases with the increase in both g_{Syn}-g_H for all the values of the synaptic thresholds (Figure 4E).

Besides the alternating bursting pattern of activity, reciprocally inhibitory circuits can produce a rich array of other outputs, depending on the underlying parameters. Thus, we classified the activity patterns of reciprocally inhibitory circuits as either silent, asymmetric, irregular spiking, antiphase bursting or antiphase spiking for each set of g_{Syn}-g_H and each value of the synaptic threshold (Figure S1, see STAR methods for the description of the classification algorithm). In the case of the escape mechanism, the circuits are typically silent or asymmetric for the parameter sets off the diagonal in the map (Figure S1 A left panels). In contrast, in the case of release, the circuits typically show either antiphase or irregular spiking pattern of activity for low values of g_{Syn} and g_H, on the border with antiphase bursting (Figure S1 A right panel). For high values of g_{Syn} and g_H, the circuit either shows antiphase bursting or asymmetric spiking (Figure S1

A, right panels), with one neuron constantly inhibiting the other one, depending on the asymmetry of neuronal intrinsic properties. The number of networks showing asymmetric firing pattern of activity is dominant on the g_{Syn}-g_H map with the intermediate value of the synaptic threshold (V_{th}=-40 mV), uncovering the differences in the excitability properties of the half-center neurons (Figure S1 middle panel). This analysis allows us to predict how the activity pattern of reciprocally inhibitory circuits will change with the change of synaptic and H conductances, depending on the mechanism of oscillation.

Effect of temperature on half-center oscillator circuits with temperature-independent synaptic and H currents

Rhythmic circuits, especially central pattern generators, must be robust to a wide range of global perturbations. Temperature is a natural and nontrivial perturbation that affects all biological processes to various degrees. We assessed the response of reciprocally inhibitory circuits relying on different mechanisms of oscillation to temperature changes. The dynamic clamp allowed us to study temperature-induced changes in the circuit output while isolating the effects of temperature on the synaptic and H currents from its effects on the cell-intrinsic currents. We built half-center oscillators with escape and release mechanisms and increased temperature in a smooth ramp from 10℃ to 20℃ (Figure 5A: release, 5B: escape). These temperatures were chosen based on the temperatures that *C. borealis* naturally experiences in the wild. In this first sets of experiments, we intentionally kept the artificial synaptic and H currents temperature-independent to explore the role of temperature-induced changes in the intrinsic properties of the cells on the circuit output.

Reciprocally inhibitory circuits with a release mechanism become less robust as the temperature increases, as evident by a significant reduction in the slow-wave amplitude and increase in irregularity in the cycle frequency (Figure 5A). 9/15 release circuits lost oscillations when the temperature was increased by 10℃. The cycle frequency of these circuits significantly increases with an increase in temperature despite no changes in the properties of synaptic or H currents (Figure 5A4,A5). On the other hand, circuits with an escape mechanism are extremely robust to an increase in temperature (Figure 5B). The cycle frequency of these circuits is remarkably stable

during the changes in temperature (Figure 5B4,B5).

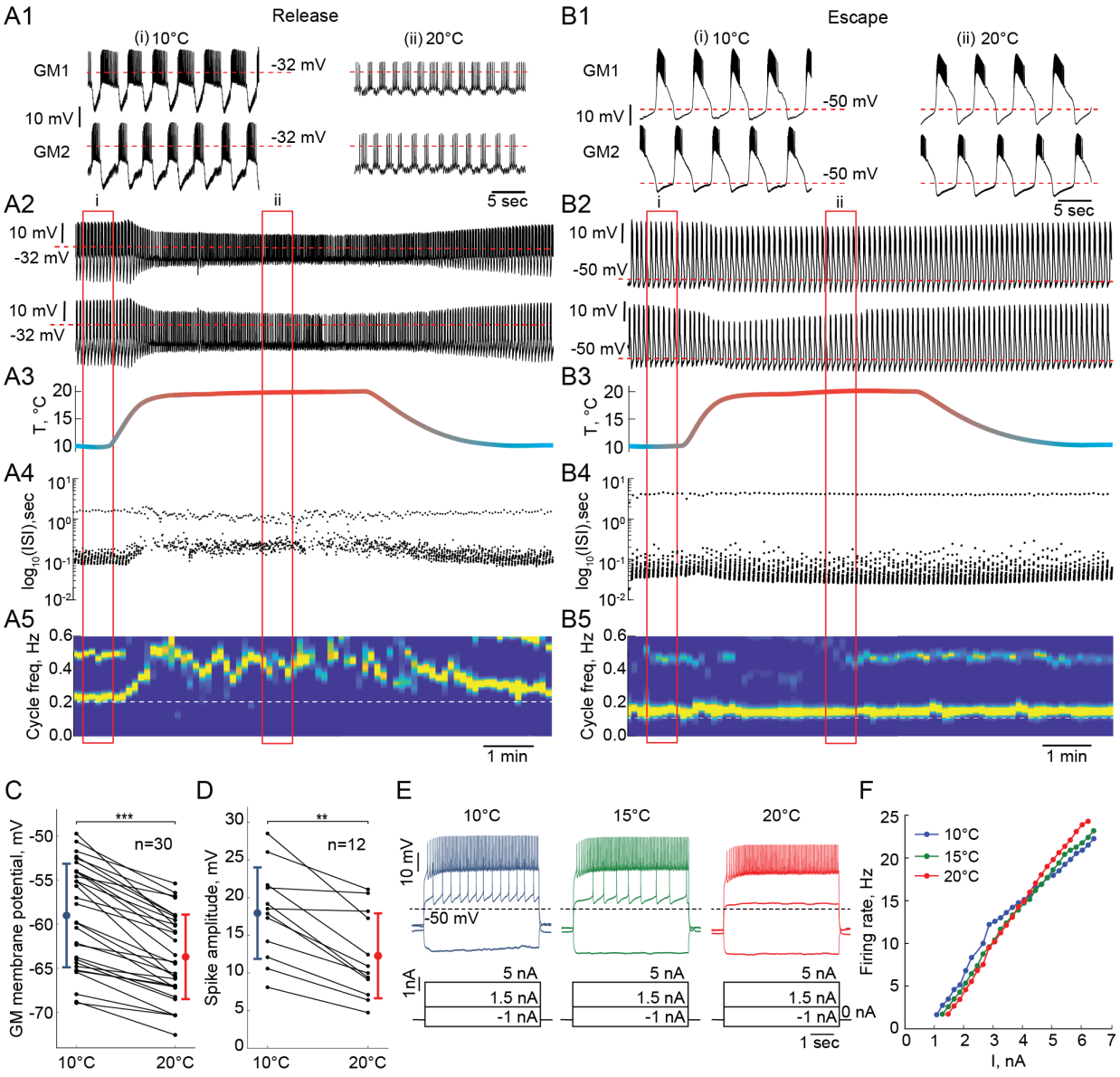

Figure 5. Response of reciprocally inhibitory circuits with release and escape mechanisms and temperature-independent artificial synaptic and H currents to an increase in temperature. A1) 25 second segments of the activity of a half-center circuit with a release mechanism at 10°C and 20°C. **A2)** Voltage traces of a half-center oscillator network in release during the increase in temperature for the entire representative experiment. **A3)** Saline temperature. **A4)** Inter spike intervals (ISI) of GM1 neuron during an increase in temperature plotted on a log scale. **A5)** Spectrogram of the GM1 voltage trace, showing an increase in oscillation frequency at high temperature. Color code represents the power spectral density, with yellow representing the maximum power and blue the minimum power. Low-frequency band with the strongest power corresponds to the fundamental frequency of the periodic signal; secondary band at higher frequency corresponds to its 2*f* harmonic. **B1-5)** Same as (A1-5) for a half-center oscillator circuit with an escape mechanism. **C)** GM resting membrane potentials at 10°C and 20°C for all the recorded neurons (n=30). Each line corresponds to one neuron, colored circles and lines correspond to means±standard deviation. Membrane potential of GM

neurons is significantly more hyperpolarized at 20°C relative to 10°C (-59.0 ± 5.87 mV at 10°C vs -63.7 ± 4.8 mV at 20°C, *** $p = 2 \cdot 10^{-6}$, Wilcoxon signed rank-sum test). **D)** GM spike amplitudes at 10°C and 20°C measured at -40 mV in response to a current step for all the neurons (n=12). The amplitude of GM spikes is significantly smaller at 20°C than at 10°C (17.9 ± 6.1 mV at 10°C vs 12.3 ± 5.6 mV at 20°C, *** $p = 0.0005$, Wilcoxon signed rank-sum test). **E)** Representative voltage traces from a single GM neuron in response to current steps recorded at 10°C (blue), 15°C (green) and 20°C (red). **F)** Frequency-current (F-I) relationships at 10°C (blue), 15°C (green) and 20°C (red) of the neuron from the representative experiment in panel (E).

Effect of temperature on the intrinsic properties of GM neurons

To explain the observed changes in the circuit output on the basis of the changes in temperature, we characterized the intrinsic properties of the GM neurons in response to changes in temperature. We measured the mean resting membrane potential of GM neurons and their responses to current steps at temperatures between $10℃$ and $20℃$. The membrane potential of GM neurons significantly hyperpolarized as temperature was increased from $10℃$ to $20℃$ (Figure 5C, n=30, $p < 0.001$, Wilcoxon signed rank-sum test). This alters the relative position of the synaptic threshold within the envelope of membrane potential oscillation that defines the oscillation mechanism.

Spike amplitude, measured at -40 mV, decreased significantly with the increase in temperature from 10°C to 20°C (Figure 5D, n=12, $p < 0.001$, Wilcoxon signed rank-sum test). This decrease in the spike amplitude decreases the robustness of half-center oscillators in a release mechanism, because at depolarized synaptic thresholds, the spikes contribute significantly to the accumulation of synaptic current. In line with this, when spikes were blocked by TTX, the range of stable alternating activity was significantly reduced and dominated by synaptic escape (Sharp et al., 1996). Finally, we measured frequency-current (F-I) relationships (n=12) and voltage-current relationships (V-I, n=9) of GM neurons between $10℃$ and $20℃$. Figure 5E shows representative voltage traces from a single GM neuron in response to current steps at $10℃$, $15℃$ and $20℃$. GM neurons required more current to initiate spiking at higher temperatures (Figure 5F). The F-I curves became steeper at higher temperatures (Figure 5F). There was no significant difference in the input resistance of GM neurons, measured by injecting negative current steps, at $10℃$ and at $20℃$ (n=10, p=0.32, Wilcoxon signed rank-sum test). The changes in the intrinsic properties of GM neurons with temperature, i.e. hyperpolarization of membrane potential and decrease in the spike amplitude, are

similar to previously reported changes in other neurons, including locust flight neurons (Xu and Robertson, 1994; Xu and Robertson, 1996), *C. borealis* Lateral Gastric (LG) neurons (Städele et al., 2015).

Taken together, a combination of two factors: a relative depolarization of the synaptic threshold due to membrane potential hyperpolarization and a decrease in the spike amplitude, cause a loss of oscillations in the circuits with a release mechanism at high temperatures. At high temperatures, the synaptic threshold becomes more depolarized than the top of the envelope of membrane potential oscillations, so that the transition between the active and inhibited states is governed by spiking activity (Figure 5A). In turn, a decrease in the spike amplitude leads to a decrease in the amplitude of the synaptic current, smaller hyperpolarization of a postsynaptic neuron, and, thus, smaller activation of H current in the postsynaptic neuron, decreasing the robustness of the oscillations. The difference in robustness of the circuits with a release mechanism is partially due to the individual variability in the sensitivity of the intrinsic properties of GM neurons to temperature changes.

While circuits with an escape mechanism that are comprised of neurons with similar intrinsic properties remain robust to an increase in temperature (Figure 5B), circuits comprised of the neurons with substantially different intrinsic excitability properties often “crash” when the temperature increases. In the intrinsic escape mechanism, the ability of the neuron to depolarize above synaptic threshold and escape their inhibition relies on its intrinsic excitability. If one of the neurons is much less excitable than the other neuron it will be constantly suppressed by the more excitable neuron, not allowing the transition between the states to happen.

The role of temperature-dependence of synapses and H current in the behavior and robustness of reciprocally inhibitory circuits

To study the effect of temperature-dependence in the parameters of the synaptic and H currents on the circuit responses to temperature, we implemented the temperature-dependence 1) only in synaptic and H conductances, 2) in both conductances and activation rates of the synaptic and H currents. Figure 6 illustrates the behavior of representative escape and release circuits in response to gradual temperature increases in all the cases, including the case of temperature-insensitive

currents for a comparison (right panels of Figure 6). The top panels of Figure 7 show the percent change in cycle and spike frequencies of the representative circuits from Figure 6. The bottom panels of Figure 7 show a summary of the effects of increasing temperature on multiple characteristics of circuit outputs across all experimental conditions (N=33). The case of temperature-independent synapses is described in detail in the previous section and is summarized in Figure 7 along with the other cases. All statistical tests, significance analyses, number of circuits/neurons and other relevant information for data comparison are provided in Tables S1-8.

$Q_{10} = 2$ for the conductances and $Q_{10} = 1$ for the activation rates of the synaptic and H currents

We set the Q_{10}, a commonly used metric describing the rate of change of a biological process due to increase in temperature by $10℃$, to 2 for the conductances of the synaptic and H currents (Figure 6B1 release, 6B2 escape). This Q_{10} value is a typical value for experimentally measured Q_{10}s in STG neurons (Tang et al., 2010). Temperature driven increase in the conductances of the synaptic and H currents increases the amplitude of oscillations, thus, making the circuits with a release mechanism more robust (Figure 6B1 voltage traces, Figure 7H). The cycle frequency of the circuits with a release mechanism decreases with an increase in temperature (Figure 6B1 spectrogram, Figure 7A,E), driven by the increases in both conductances in accordance with the findings shown in the right panel of Figure 3B. On average, temperature-dependence in the synaptic and H conductances makes circuits with a release mechanism more robust to temperature increase. However, when circuits were comprised of neurons with substantially different intrinsic properties, the decrease in the on-off transition frequency led to unstable oscillations.

The cycle frequency of the circuits with an escape mechanism remains constant over the whole temperature range (Figure 6B2 spectrogram, Figure 7B,E), similar to the case of temperature-independent synapses. Temperature-induced increases in the synaptic and H conductances counteract each other in the case of the escape mechanism as illustrated in the left panel of Figure 3B, (i.e. the frequency is conserved along the diagonal of g_H-g_{Syn} map). The spike frequency and number of spikes per burst

of the circuits with either release of escape mechanisms significantly increase from 10℃ to 20℃ (Figure 7C,D,H).

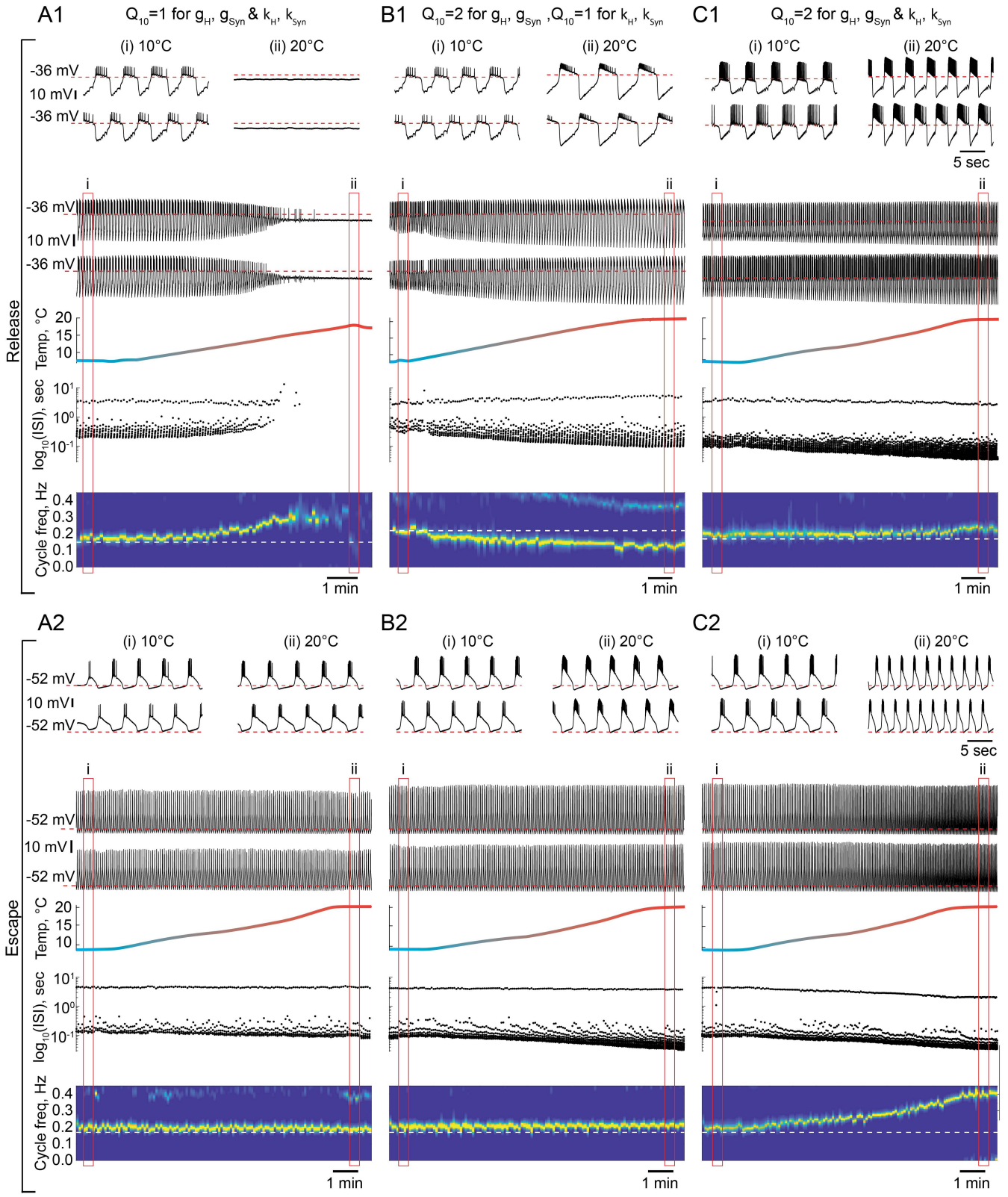

Figure 6. The role of temperature dependence in the synaptic and H currents in the response of the circuits with release and escape mechanisms to changes in temperature. **A1)** Representative example of the behavior of a half-center oscillator in release in case of temperature-independent synaptic and H conductances and activation rates of these currents (g_H, g_{Syn}, k_H, K_{Syn} Q_{10}=1). Figure follows the same format as figure 5A-B. **A2)** Same condition as in (A1) for a circuit in escape. **B1)** Representative example of the behavior of a half-center oscillator in release in case of temperature-dependence of the synaptic and H conductances with a Q_{10}=2 and temperature-independent activation rates (k_H, K_{Syn} Q_{10}=1). **B2)** Same condition as in (B1) for a circuit in escape. **C1)** Representative example of the behavior of a half-center oscillator in release in case of temperature-dependence of the synaptic and H conductances and activation rates with a Q_{10}=2. **C2)** Same condition as in (C1) for a circuit in escape.

$Q_{10} = 2$ for the conductances and the activation rates of the synaptic and H currents

We next implemented temperature-dependence in both the conductances and activation rates of the synaptic and H currents by setting these $Q_{10}s$ to 2. Both, escape and release circuits were most robust to the changes in temperature in this case, due to the increase in the amplitude of the oscillations and faster transitions between the on-off states (Figure 6C1 release, C2 escape). Although both circuits were bursting robustly during the entire temperature range, there was a significant difference in the frequency responses of the escape and release circuits. Across all experiments, the cycle frequency of the circuit with a release mechanism did not significantly change over $10℃$ (Figure 6C1 spectrogram, Figure 7E), while the cycle frequency of the circuits with an escape mechanism increased dramatically (Figure 6C2 spectrogram, Figure 7H). In release, an increase in cycle frequency governed by changes in the intrinsic properties of the neurons and by an increase in the activation rates of synaptic and H currents was counteracted by a decrease in cycle frequency governed by an increase in synaptic and H conductances. Combination of these processes keeps the cycle frequency of release circuits nearly constant throughout the temperature ramp. In escape, an increase in cycle frequency is mostly driven by an increase of the activation rate of H current. The spike frequency and the oscillation amplitude of circuit with either release or escape mechanisms significantly increased over $10℃$, similar to the case of $Q_{10} = 2$ for conductances only (Figure 7C,D,F). The number of spikes per burst of the escape circuits did not significantly change with the increase in temperature, unlike in the release circuits (Figure 7G).

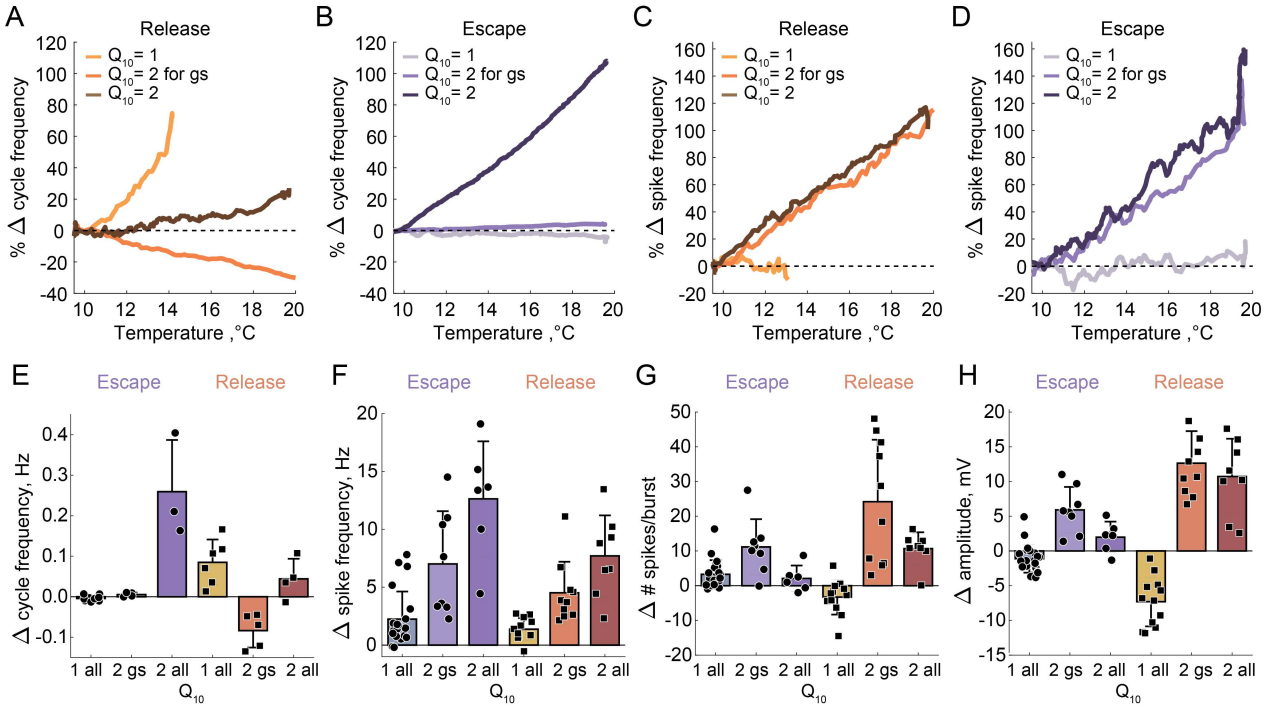

Figure 7. Summary of the effects of temperature on the characteristics of half-center oscillators with escape and release mechanisms and different temperature-dependences in the synaptic and H currents. A) Percent change in cycle frequency of the release circuits shown in Figure 6 with an increase in temperature from 10°C to 20°C. **B)** Percent change in cycle frequency of the escape circuits shown in Figure 6 with an increase in temperature from 10°C to 20°C. **C)** Percent change in spike frequency of the release circuits in Figure 6 with an increase in temperature from 10°C to 20°C. **D)** Percent change in spike frequency of the escape circuits in Figure 6 with an increase in temperature from 10°C to 20°C. **E)** Change in cycle frequency with an increase in temperature from 10°C to 20°C across all experimental conditions (N=33). **F)** Change in spike frequency across all experimental conditions. **G)** Change in number of spikes per burst across all experimental conditions. **H)** Change in slow-wave amplitude across all experimental conditions.

Different characteristics of the circuit output are differently sensitive to temperature increase depending on the mechanism of oscillation and $Q_{10}s$ of the synaptic and ionic currents. The duty cycle was relatively independent of variations in temperature in all the cases (Tables S1-2). To assess whether temperature affects the mechanism of oscillation we calculated the change in ERQ over $10℃$ for different Q_{10} cases (Table S1,8). ERQ did not significantly change for the release circuits. ERQ became significantly more positive for the escape circuits with temperature-independent synaptic and H currents, indicating the change in the mechanism of oscillation towards release with the increase in temperature. An example of the change in the mechanism of oscillation from escape at $10℃$ all the way to release at $20℃$ is shown in Figure S2. During the transition, the half-center exhibited characteristics of both mechanisms with

various balances between the mechanisms at different temperatures. The cycle frequency remained constant for a wide range of temperatures until the on-off transitions in the circuit were dominated by the synaptic release mechanism (Figure S2E).

Effect of a neuromodulatory current on the robustness of circuits with release and escape mechanisms

A number of neurotransmitters and peptides converge on an inward current with the same voltage dependence, known as I_{MI} (Swensen and Marder, 2000, 2001). To explore the effect of I_{MI} on reciprocally inhibitory circuits with different mechanisms of oscillation, we injected artificial I_{MI} via the dynamic clamp into both neurons comprising half-center oscillators (Figure 8A) and varied the synaptic threshold to alter the mechanism. Figure 8B illustrates representative recordings of a half-center oscillator at three different synaptic thresholds corresponding to escape, mixture, and release mechanisms in control (black traces) and with the addition of I_{MI} (blue traces). We calculated the frequency of oscillations as a function of the synaptic threshold in control and with the addition of I_{MI} (g_{MI} =150 nS). Figure 8C shows this relationship for the representative experiment in panel B. I_{MI} produced no effect on the cycle frequency of escape circuits, while I_{MI} decreased the cycle frequency of the circuits with a mixture of mechanisms or in release. Addition of I_{MI} increased the robustness of circuits with a release mechanism, increasing the amplitude of oscillations (Figure 8B, right most traces) and expanding the range of synaptic thresholds producing stable antiphase bursting pattern of activity (Figure 8C). At the same time, I_{MI} made oscillations less stable and irregular for circuits operating with a mixture of mechanisms. This is obvious in the amplified asymmetry between the units comprising the circuit (Figure 8B middle traces), an increase in the standard deviation of the cycle frequency and a break in the central region of the cycle frequency curve corresponding to a mixed regime (Figure 8C).

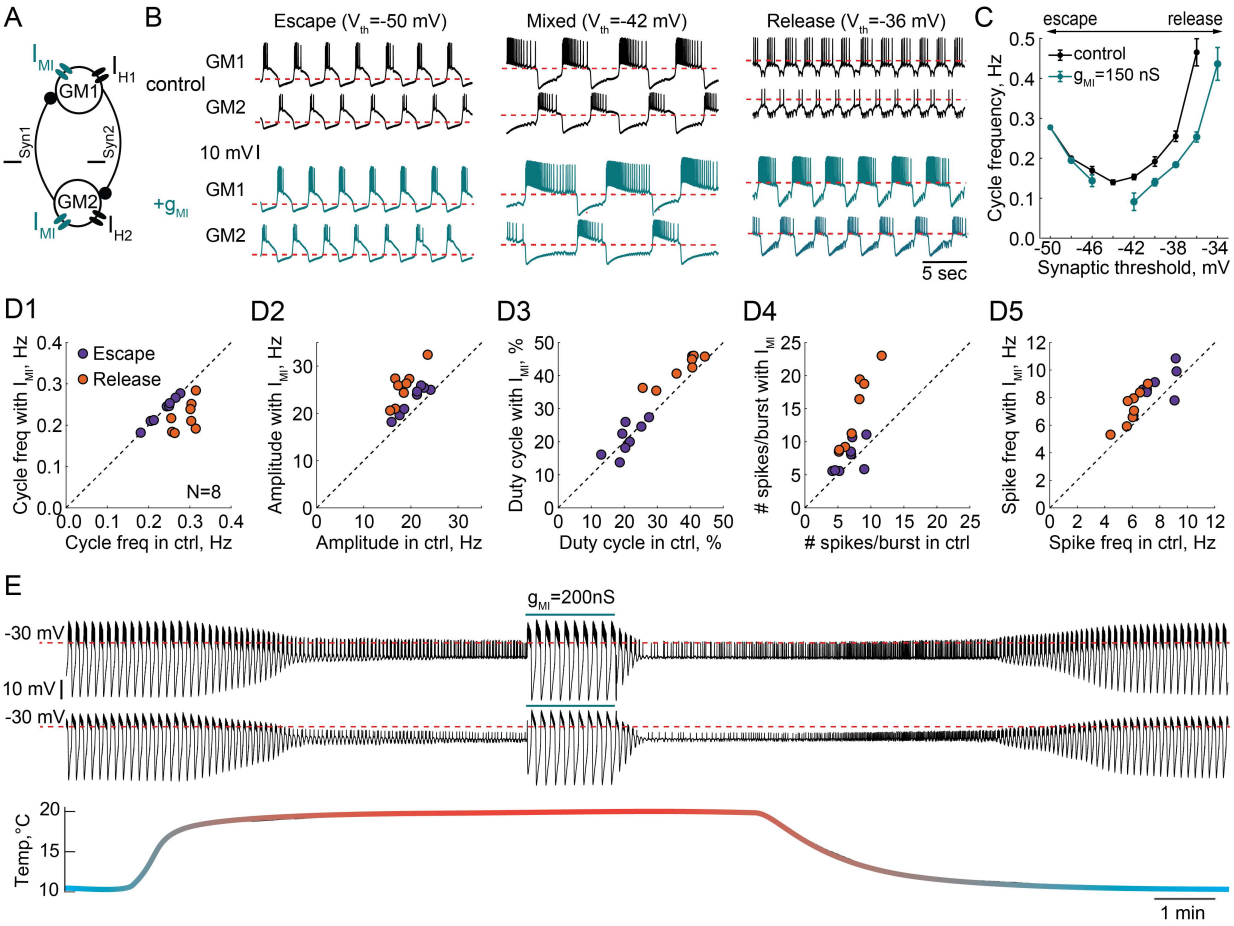

Figure 8. Effect of a modulatory current (I_{MI}) on the behavior of reciprocally inhibitory circuits with different oscillatory mechanisms. A) A schematic representation of a reciprocally inhibitory circuit with a dynamic clamp modulatory current (I_{MI}). **B)** Representative traces of a half-center oscillator for different synaptic thresholds in control (black) and with the addition of I_{MI} (g_{MI}=150 nS, blue). **C)** Oscillation frequency of the circuit in panel B as a function of the synaptic threshold in control (black) and with the addition of I_{MI} (blue). **D)** Characterizing the half-center oscillator output in escape and release with the addition of I_{MI} (N=8). **D1)** Cycle frequency (Escape: 0.236 ± 0.033 Hz in control vs 0.237 ± 0.032 Hz with $I_{MI,}$ n.s. p=0.38, paired-sample t-test; Release: 0.289 ± 0.026 Hz in control vs 0.22 ± 0.036 Hz with $I_{MI,}$ *** p=0.0003, paired-sample t-test). **D2)** Slow-wave amplitude (Escape: 20.5 ± 2.8 mV in control vs 23.0 ± 2.9 mV with $I_{MI,}$ *** p<0.0001, paired-sample t-test; Release: 18.4 ± 2.5 mV in control vs 25.7 ± 3.8 mV with $I_{MI,}$ *** p<0.0001, paired-sample t-test). Amplitude increase in release is significantly larger than in escape, *p=0.02, paired-sample t-test. **D3)** Duty cycle (Escape: 20.8 ± 4.3 % in control vs 21.1 ± 4.9 % with $I_{MI,}$ n.s. p=0.8, paired-sample t-test; Release: 37.3 ± 6.5 % in control vs 42.2 ± 4.3 % with $I_{MI,}$ *p=0.002, paired-sample t-test). **D4)** Number of spikes per burst (Escape: 6.7 ± 1.9 in control vs 7.6 ± 2.3 with $I_{MI,}$ n.s. p=0.2, paired-sample t-test; Release: 7.6 ± 2.2 in control vs 14.4 ± 5.7 with $I_{MI,}$ **p=0.001, paired-sample t-test). **D5)** Spike frequency (Escape: 7.8 ± 1.2 Hz in control vs 8.7 ± 1.3 Hz with I_{MI}, *p=0.029, paired-sample t-test; Release: 6.0 ± 0.8 Hz in control vs 7.2 ± 1.3 Hz with $I_{MI,}$ **p=0.001, paired-sample t-test). **E)** I_{MI} restores the oscillations in the circuit with a release mechanism that stopped oscillating at high temperature. Example voltage traces of a half-center oscillator circuit in release during an increase in temperature from 10°C to 20°C. In this example, synaptic and H conductances and activation rates are temperature-independent.

We quantified the change in cycle frequency, oscillation amplitude, duty cycle, spike frequency and number of spikes per burst across both neurons in circuits with the addition of modulatory current (N=8, Figure 8D1-5). The cycle frequency of escape circuits did not change with the addition of I_{MI} but significantly decreased in release circuits (Figure 8D1). I_{MI} increased the amplitude of oscillations in both modes, with a significantly larger increase in release (Figure 8D2), making the oscillations more robust. The duty cycle of the circuits in escape was statistically invariant to modulation, while there was a small but statistically significant increase in the duty cycle of the circuits in release (Figure 8D3). The number of spikes per burst significantly increased with I_{MI} in release but not escape (Figure 8D4). Finally, I_{MI} produced a small but statistically significant increase in the frequency of the spikes within bursts for both types of circuits (Figure 8D5). Overall, across all the characteristics, circuits with a release mechanism were significantly more sensitive to a modulatory current than circuits with an escape mechanism.

These observations suggest that the same type of modulation can produce vastly different effects on the output of a circuit depending on the underlying mechanism of oscillation, and can make a circuit more or less robust to subsequent perturbations, potentially changing its sensitivity to pharmacological agents. For example, I_{MI} increases the robustness of the circuit perturbed by an increase in temperature (Figure 8E). I_{MI} restored the antiphase oscillations in a release circuit at high temperature, by depolarizing the neurons over the synaptic threshold and increasing the amplitude of oscillations. This is similar to the neuromodulatory rescue of the temperature-induced cessation of the gastric mill rhythm (Städele et al., 2015). This could be one of the mechanisms by which neuromodulators improve circuit robustness.

Discussion

One of the most difficult problems facing systems neuroscience is to determine the mechanisms that generate a given circuit output. The present work is designed to provide some fundamental insights into that problem, by studying a purposefully simple rhythmic circuit. Because some of the circuit parameters are constructed with the dynamic clamp, and are therefore known, we have been able to gain insight into how circuits that appear similar in function can respond differently to the same perturbations. In dynamic clamp hybrid circuits, we have access to some of the hidden variables that define the dynamical mechanisms governing circuit behavior. At the same time, we have not sacrificed the complexity of the biological neurons. This allowed us to study how the interaction between biophysical and dynamical properties of these neural circuits define their robustness. The findings of this paper have implications for understanding animal-to-animal variability in circuit responses to various stressors and modulators.

Unperturbed half-center circuits with escape and release mechanisms can have very similar characteristics, including burst and spike frequencies. Thus, if the mechanism is not known *a priori*, it is impossible to identify the underlying mechanisms of circuit function from the baseline spiking activity. One way to reveal hidden differences in the mechanism underlying circuit dynamics is by perturbing them. We showed that reciprocally inhibitory circuits with different underlying oscillation mechanisms are not equally robust to perturbations. Particularly, circuits in release mode are robust to variations in synaptic and H conductances, but sensitive to an increase in temperature and modulation. In contrast, the circuits in escape rely on tight correlations between synaptic and H conductances to generate robust bursting but are resilient to increases in temperature and modulation.

Previous computational studies showed that half-center oscillators relying on either release or escape mechanisms differentially respond to synaptic inputs and current pulses (Daun et al., 2009, Zhang and Lewis, 2013). Daun et al. (2009) used model neurons with or without persistent sodium current to form half-center oscillators. When asymmetric noise was injected into only one of the neurons, half-centers operating in escape had a larger range of oscillation period than did circuits with release

or a mixture of mechanisms (Daun et al., 2009). Additionally, half-centers built with two Morris-Lecar model neurons have significantly different phase response properties and phase locking dynamics depending on whether they operate in escape or release (Zhang and Lewis, 2013).

Model half-center circuits are typically built with two identical neurons, although experimental data suggest that the conductance values and intrinsic properties of neurons even of the same type can differ significantly (Doloc-Mihu and Calabrese, 2014; Goldman et al., 2001; Marder and Goaillard, 2006; Prinz et al., 2003; Prinz et al., 2004; Roffman et al., 2012; Schulz et al., 2006; Schulz et al., 2007; Srikanth and Narayanan, 2015; Swensen and Bean, 2005; Temporal et al., 2012; Tobin et al., 2009; Tran et al., 2019). The studies in which the dynamic clamp is used to create half-center circuits from biological neurons profit from natural cell-to-cell and animal-to-animal variability to investigate circuit responses to stressors and modulators. For example, Grashow et al. (2009) found that the application of either serotonin or oxotremorine (a muscarinic receptor agonist) on average increased the oscillation frequency and made alternating bursting more robust by extending the parameter range over which bursting exists. However, there was a substantial variability in individual responses of half-center circuits to neuromodulation, with a few circuits showing “anomalous” decreases in cycle frequency in the presence of modulators. Based on the results of the present study, some of the variability in Grashow et al. (2009) is likely due to the differences in underlying mechanisms of oscillations across the circuits and the degree of asymmetry between the units comprising the circuit. We show that the same neuromodulatory current can either have no effect on the same circuit if operating in escape, destabilize the circuits if operating in mixed mode or increase the robustness of the circuit if operating in release (Figure 8). Thus, knowing the dynamical mechanism involved in generating the circuit output is crucial for understanding the circuit responses to stimuli.

A similar variability in the response to a neuromodulator is seen in the crustacean gastric mill rhythm. This rhythm is generated by a half-center oscillator and can be elicited by multiple mechanisms (Powell et al., 2021b). Stimulation of the MCN1 projection neuron or bath-applying the peptide CabPK result in gastric mill rhythms with similar output patterns (Powell et al., 2021b). Despite the similarity of their baseline

activity patterns, these rhythms rely on participation of different neurons and respond differently to hormone CCAP, which is known to activate I_{MI} (Swensen and Marder, 2000, 2001). CCAP, slows down MCN1-generated rhythm, but, in contrast, speeds up CabPK-generated rhythm (Kirby and Nusbaum, 2007; Powell et al., 2021b). We propose that the MCN1 rhythm might operate in release, while CabPK-rhythm operates in escape. Thus, different modulators can elicit different dynamical mechanisms of rhythm generation. In support of this hypothesis, it has been reported that similar gastric mill rhythms, which are generated by a stimulation of disparate neuromodulatory pathways, have different temperature sensitivity (Städele et al., 2015; Powell et al., 2021a). A modest temperature increase of $3℃$ abolishes the MCN1-rhythm (Städele et al., 2015), in contrast, the VCN-rhythm is temperature-robust over a wide range of temperatures, between $7℃$ and $25℃$ (Powell et al., 2021a). We propose that the difference in temperature sensitivity between the two versions of the gastric mill rhythm could be explained by the differences in their dynamical mechanisms of oscillation.

Many studies found significant correlations between the conductances of voltage-dependent currents in both invertebrates and vertebrates (Amendola et al., 2012; Calabrese et al., 2011; Goaillard et al., 2009; Khorkova and Golowasch, 2007; Schulz et al., 2006; Schulz et al., 2007). It has been argued that reliable circuit output and resilience to perturbations are enhanced by the conductance correlations, rather than by the particular values of individual parameters (Olypher and Calabrese, 2007; Onasch and Gjorgjieva, 2020; Tobin et al., 2009; Zhao and Golowasch, 2012). In line with this, we found that synaptic and H conductances are positively correlated in the circuits with escape mechanisms (Figure 3A), contributing to the robustness of these circuits to variations in temperature. Changes in the synaptic and H conductances with temperature counteract each other keeping the frequency of oscillations stable for a wide range of temperatures (Figure 6 B2).

Because temperature differentially affects many nonlinear processes shaping circuit output, it is a nontrivial challenge for a circuit to maintain its function over a wide range of temperatures. Despite that, many neuronal circuits, including the pyloric and half-center driven gastric mill circuits of crustaceans, are temperature compensated and function over an extended physiological temperature range (Haddad and Marder, 2018;

Kushinsky et al., 2019; Powell et al., 2021a; Soofi et al., 2014; Tang et al., 2010; Tang et al., 2012). Complicating the situation, circuit robustness to temperature is strongly influenced by the modulatory environment (Haddad and Marder, 2018; Soofi and Prinz, 2015; Städele et al., 2015). Obtaining insights into the mechanisms that underly acute temperature robustness is difficult. Temperature is a particularly difficult perturbation to model in biologically plausible circuits because there are many free parameters to set, as temperature affects both the conductances and activation rates of the currents, making it a highly unconstrained problem. Because it is difficult to measure the temperature dependence of all of the currents in a given cell type (Tang et al., 2010), most modeling studies (Alonso and Marder, 2020; Caplan et al., 2014; O'Leary and Marder, 2016; Rinberg et al., 2013) employ Q_{10} values that are only partially based on measured values. In simplified models it is possible to study the dynamical mechanisms of robustness and characterize bifurcations as a function of temperature (Rinberg et al., 2013), but many biophysical details are lost. In contrast, in the hybrid neural-computer dynamic clamp circuits studied in this paper, we can control the dynamical mechanisms governing circuit behavior and temperature-dependence in the computer-generated parameters, without making any assumptions about the temperature dependence of the intrinsic currents of the neurons. Thus, we benefit from not having to over-simplify the effects of temperature on the biological neurons.

It is as of yet unclear whether circuits that depend on one or another dynamical mechanism for operation are intrinsically more robust to all perturbations, or whether robustness is determined idiosyncratically for each circuit configuration and perturbation. The present study illustrates how nontrivial it is to explain circuit function on the basis of basal firing pattern alone. The dynamical mechanisms underlying half-center oscillator transitions are well defined in modeling studies that reveal the underlying interactions between hidden state variables and voltage-dependent synaptic and intrinsic currents. While theoretical studies provide mechanistic insight, it can be quite difficult to establish how those mechanisms are instantiated in biological neurons. Moreover, virtually all previous computational studies in half-centers were done with identical neurons, and in no case will two or more biological neurons even of the same cell type, be identical. The dynamic clamp studies here provide access to some of the

729 fundamental dynamical mechanisms important for generation of antiphase oscillations,
730 while retaining the intrinsic “features” of the biological neurons. In conventional current
731 clamp experiments the investigator does not have a continuous access to state
732 variables of the currents, while in the dynamical clamp experiments state variables of
733 the computer-generated currents are readily accessible. A fundamental conclusion of
734 this work is that very nuanced changes in circuit mechanism can profoundly alter the
735 circuit robustness to perturbations and inputs. Thus, a challenge for the future will be
736 developing new methods to extract dynamical mechanisms underlying circuit function
737 from biological circuits while they are in operation.
738
739 **Acknowledgments**
740 Support: NIH National Institute of Health grant 2 R01 MH046742, and the Swartz
741 Foundation (E.O.M).
742
743 **Author contributions**
744 E.O.M. and E.M. designed the experiments, E.O.M and P.N. performed the experiments
745 and data analysis. E.O.M wrote the manuscript, and all authors edited the manuscript.
746
747 **Declaration of interests**
748 The authors declare no competing interests.
749
750
751
752
753
754
755

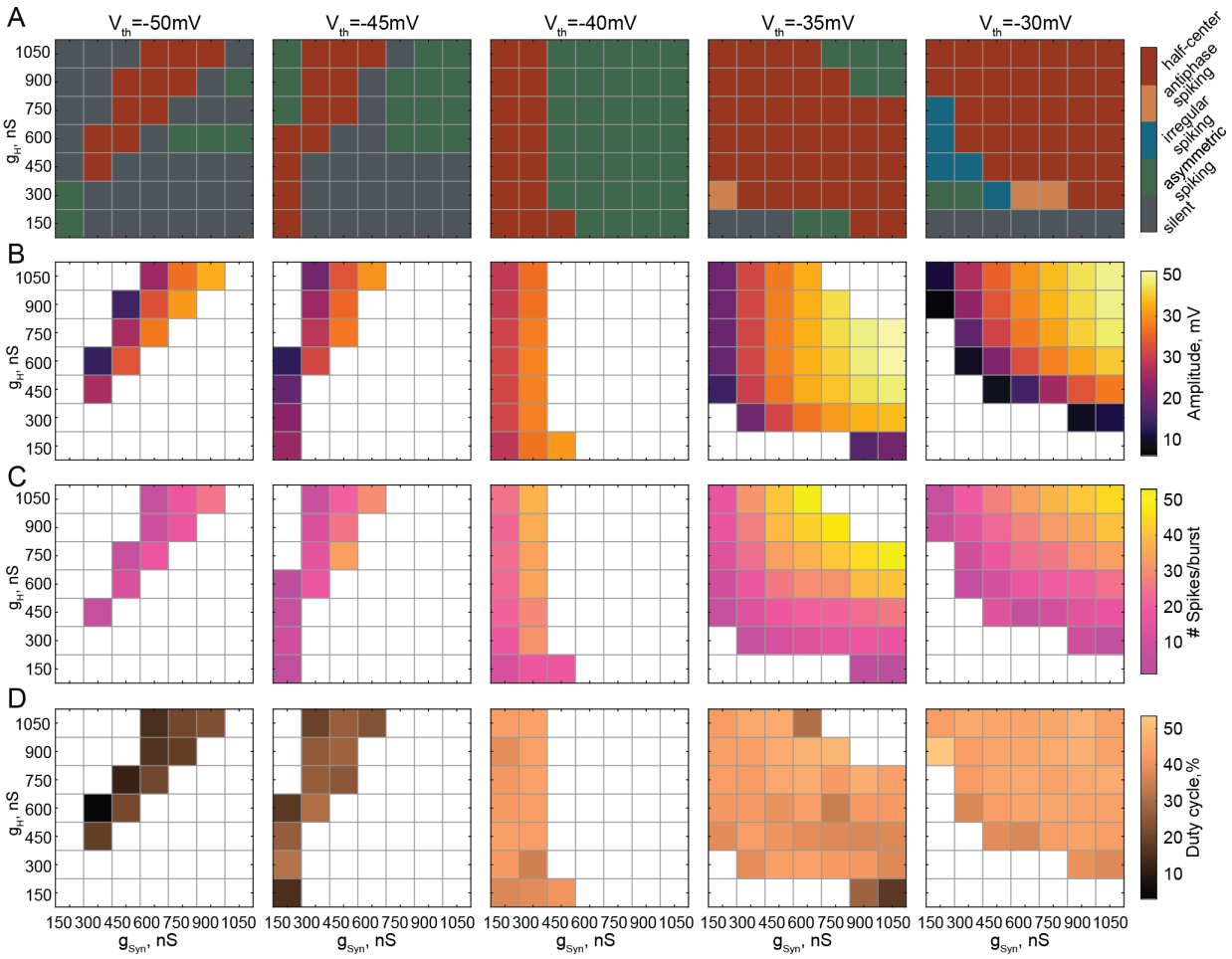

Figure S1. **Supplementary figure for figure 4. A)** Activity patterns of reciprocally inhibitory circuits for different combinations of g_{Syn} and g_H and the synaptic thresholds of -50 mV, -45 mV, -40 mV, -35 mV and -30 mV. **B)** Dependence of the oscillation amplitude on g_{Syn} and g_H for different synaptic thresholds. **C)** Dependence of the number of spikes per burst on g_{Syn} and g_H for different synaptic thresholds. **D)** Dependence of the duty cycle on g_{Syn} and g_H for different synaptic thresholds.

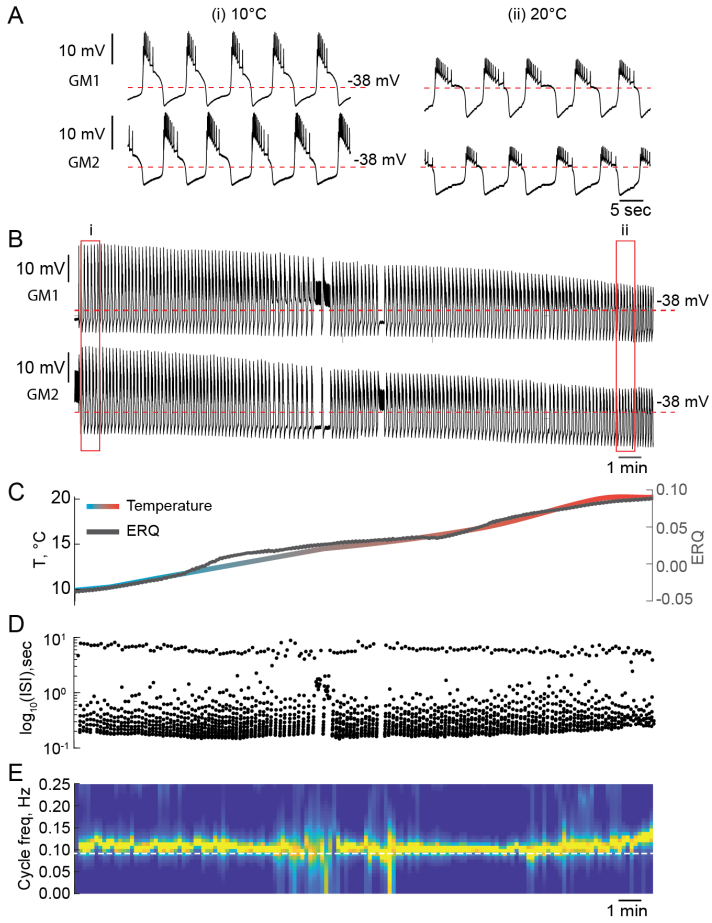

Figure S2. Temperature can alter the mechanism of oscillations of reciprocally inhibitory circuits. A) 1 min segments of the activity of a half-center oscillator recorded at 10°C and 20°C. **B)** Voltage traces of a half-center oscillator during the temperature ramp from the entire experiment. **C)** Temperature ramp and corresponding ERQ. Increase in temperature switches the mechanism of oscillations from a mixture of intrinsic and synaptic escape to synaptic release. **D)** Inter spike intervals (ISI) of GM1 neuron during the increase in temperature plotted on a log scale. **E)** Spectrogram of the GM1 voltage trace.

764

METHODS

RESOURCE AVAILABILITY

Lead contact

Further information and requests for resources should be directed to the Lead Contact, Ekaterina Morozova (morozova.e.o@gmail.com).

Materials availability

This study did not generate any new unique reagents.

Cancer Borealis crabs used in this study are available from Commercial Lobster (Boston, MA)

Data and code and availability

Data will be publicly available upon publication.

Custom RTXI modules are available on GitHub (https://github.com/eomorozova/half_center_oscillator_rtxi_module)

All the analysis scripts are available on GitHub (https://github.com/eomorozova/hco-analysis).

Any additional information required to reanalyze the data reported in this paper is available from the lead contact upon request.

EXPERIMENTAL MODEL AND SUBJECT DETAILS

Adult male Jonah Crabs, *Cancer borealis*, (N=43) were obtained from Commercial Lobster (Boston, MA) and maintained in artificial seawater at 10-12˚C in a 12-hour light/dark cycle. On average, animals were acclimated at this temperature for one week before use. Prior to dissection, animals were placed on ice for at least 30 minutes. Dissections were performed as previously described (Gutierrez and Grashow, 2009). In short, the stomach was dissected from the animal and the intact stomatogastric nervous system (STNS) was removed from the stomach including the commissural ganglia, esophageal ganglion and stomatogastric ganglion (STG) with connecting motor nerves. The STNS was pinned in a Sylgard-coated (Dow Corning) dish and continuously superfused with saline. Saline was composed of 440 mM NaCl, 11 mM KCl, 26 mM $MgCl_2$, 13 mM $CaCl_2$, 11 mM Trizma base, 5 mM maleic acid, pH 7.4 –7.5 at 23°C (~7.7–7.8 pH at 11°C).

METHOD DETAILS

Electrophysiology

Intracellular recordings from the somata of gastric mill (GM) neurons were made using two-electrode current clamp in the desheathed STG with 10–20 MΩ sharp glass microelectrodes filled with 0.6 M K_2SO4 and 20 mM KCl solution (Figure 1A). Intracellular signals were amplified with an Axoclamp 900A amplifier (Molecular Devices, San Jose). Extracellular nerve recordings were made by building wells around nerves using a mixture of Vaseline and mineral oil and placing stainless-steel pin electrodes within the wells to monitor spiking activity. Extracellular nerve recordings were amplified using model 3500 extracellular amplifiers (A-M Systems). Data were acquired using a Digidata 1440 digitizer (Molecular Devices, San Jose) and pClamp data acquisition software (Molecular Devices, San Jose, version 10.5) and Real-Time eXperiment Interface (RTXI) software (http://rtxi.org/) version 2.2 or 1.4. Recordings were done with a sampling frequency of 10 kHz. For identification of GM neurons, somatic intracellular recordings were matched to action potentials on the dorsal gastric nerve (*dgn*), and/or the anterior lateral nerve (*aln*).

For the process of blocking descending modulatory inputs to the STG, a Vaseline well was built around the exposed portion of the *stn*. Propagation of axonal signaling, and, thus, neuromodulatory release, was blocked from upstream ganglia by replacing saline in the Vaseline well with 10^{-7}M tetrodotoxin (TTX) in a 750 mM sucrose solution. 10^{-5}M Picrotoxin (PTX) was used to block inhibitory glutamatergic synapses (Marder and Eisen, 1984). Preparations were allowed to stabilize after decentralization and PTX application for at least 1 hour prior to building a reciprocally inhibitory circuit via dynamic clamp.

Dynamic clamp

To create the half-center oscillator circuits, artificial reciprocal inhibitory synaptic currents (I_{Syn}) and hyperpolarization-activated inward currents (I_H) were added via the dynamic clamp, following the methods described in Sharp et al (1996)(Figure 1). Simulation of voltage-dependent currents in real time was done using Real-Time eXperimental Interface (RTXI 2.2 or 1.4) (http://rtxi.org/) (Patel et al., 2017). Custom RTXI modules were written using the programming language C++.

826 The synaptic current is given by the following expression:

827 $$I_{syn} = g_{syn} \cdot s(V_{pre}) \cdot (V_{post} - E_{syn}), \qquad (1 - s_\infty)\frac{ds}{dt} = \frac{s_\infty - s}{\tau_{syn}}$$

828 where V_{pre} and V_{post} are presynaptic and postsynaptic voltages, s is the synaptic gating
829 varible, s_∞ is the steady-state synaptic activation, given by a sigmoidal function
830 $s_\infty = \frac{1}{1+e^{\frac{V-V_{th}}{V_{slope}}}}$ (Figure 1B, purple and orange curves).

831 The hyperpolariztion-activated inward current is described in Buchholtz et al
832 (1992):

833 $$I_H = g_H \cdot r(V_{post}) \cdot (V_{post} - E_H), \qquad \frac{dr}{dt} = \frac{r_\infty - r}{\tau_H},$$

834 where r is the gating varible of H current, r_∞ is the steady-state activation, given by a
835 sigmoidal function $r_\infty = \frac{1}{1+e^{\frac{V-V_{1/2}}{S_r}}}$ (Figure 1B, black curve), τ_r is the voltage-dependent
836 time constant given by $\tau_H = \frac{\tau_{H0}}{1+e^{\frac{V-V_{\tau_r}}{S\tau_r}}}$.

837 In a subset of experiments we simulated inward neuromodulatory current (I_{MI}) via
838 dynamic clamp (Swensen and Marder, 2001):

839 $$I_{MI} = g_{MI} \cdot m \cdot (V_{post} - E_{MI}), \qquad \frac{dm}{dt} = \frac{m_\infty - m}{\tau_m},$$

840 where m is the gating varible of neuromodulatory current, m_∞ is the steady-state
841 activation, given by a sigmoidal function $m_\infty = \frac{1}{1+e^{\frac{V-V_{MI_{1/2}}}{S_{MI}}}}$.

842 Parameter values of the currents injected in both neuron were the same to
843 preserve the symmetry and are given in Table 1. Since the artificial currents injected
844 into both neurons had the same parameter values, in order to create stable half-center
845 oscillators, neurons used to comprised the oscillator had to have similar resting
846 membrane potentials and intrinsic excitability. Thus, in the sunset of experiments, when
847 two GM neurons had very different resting membrane potentials at baseline, the
848 membrane potential were brought to the same range of $\pm 5\ mV$ by either injecting a
849 small amout of positive constant current or negative leak current to a more
850 hyperpolarized cell.

Table 1. Parameter values for the dynamic clamp

Parameter	Value	Description
Synaptic current (I_{syn})		
g_{syn}	Varied from 150 to 1050 nS	Maximal conductance of synaptic current
E_{syn}	-80 mV	Reversal potential of synaptic current
V_{th}	Varied from -28 to -54 mV	Synaptic threshold voltage
τ_{syn}	50 or 100 msec	Synaptic time constant
V_{slope}	-2 mV	Slope factor of synaptic activation function
Hyperpolarization-activated inward current (I_H)		
g_H	Varied from 150 to 1050 nS	Maximal conductance of H current
E_H	-10 mV	Reversal potential of H current
$V_{1/2}$	-50 mV	Half-maximal activation voltage of H current
s_r	7 mV	Slope factor of H current activation function
τ_{H0}	2000 or 3000 msec	Time constant of H current
V_{τ_r}	-110 mV	Half-maximal voltage of H current time constant
s_{τ_r}	-13 mV	Slope factor of H current time constant
Neuromodulatory inward current (I_{MI})		
g_{MI}	100, 150 or 200 nS	Maximal conductance of neuromodulatory current
E_{MI}	-20 mV	Reversal potential of neuromodulatory current
$V_{MI_{1/2}}$	-21 mV	Half-maximal activation voltage of I_{MI}
τ_m	4 msec	Time constant of neuromodulatory current
s_{MI}	-8 mV	Slope factor of I_{MI} activation function

Temperature experiments

Temperature of the superfusing saline was controlled using either a waveform generator (RIGOL, DG1022 series) or Arduino connected to a temperature controller (model CL-100, Warner Instruments) and altered during each experiment using a Peltier device and thermocouple (SC-20 and TA-29, Warner Instruments). We performed three types of temperature experiments. In the first set of experiments temperature was changed in one big step from 10ºC to 20ºC in 1 minute, held at 20ºC for 2-10 min and brought back to 10ºC in one step (N=13). In the second set of temperature experiments, waveform generator or Arduino were programmed to change temperature from 10ºC to 20ºC in 2ºC/minute steps (N=5). Each temperature step was held for 6 min during which synaptic threshold was changed via RTXI from -50 mV to -30 mV in 5 mV/min steps to explore the effect of temperature on half-center oscillator circuit with different oscillatory mechanisms. In the final set of temperature experiments, waveform generator or Arduino was programmed to generate a smooth temperature ramp from 10ºC to 20ºC

over 10 to 20 minutes (N=22). Temperature was then held for 2-5 minutes at 20°C and gradually brought back to 10°C in a symmetric ramp. For a subset of temperature experiments (N=15) inward neuromodulatory current I_{MI} was simulated via dynamic clamp in both GM neurons at either 10°C, 20°C or both temperatures.

Temperature dependence of the conductances and time constants of the currents generated with the dynamic clamp was implemented in the following way: $g_{syn} = g_{syn0} \cdot Q_{10}^{\frac{T-T_0}{10}}$, $g_H = g_{H0} \cdot Q_{10}^{\frac{T-T_0}{10}}$, $\tau_{syn} = \frac{\tau_{syn0}}{Q_{10}^{\frac{T-T_0}{10}}}$, $\tau_H = \frac{\tau_{H0}}{Q_{10}^{\frac{T-T_0}{10}}}$, where T is the saline temperature and $T_0 = 10℃$ is a reference temperature. Q_{10}, a metric describing the rate of change of a biological process due to increase in temperature by 10°C, was set to either 1 or 2, according to experimentally measured $Q_{10}s$ in STG neurons (Tang et al., 2010).

QUANTIFICATION AND STATISTICAL ANALYSIS

Spike detection

Spikes were detected using local maxima detection algorithm in MATLAB, using a threshold of -40 mV and a peak prominence (height of the peak above the reference level) of 3. Prior to running local maxima algorithm voltage traces were smoothed using moving average filter with 10 data points for calculating smoothed value to reduce the noise in the traces.

Burst detection

For an accurate detection of the bursts we used two methods: based on the spiking activity and based on the slow wave, as in most cases circuits exhibited prominent slow wave during alternating bursting.

Burst detection based on the spiking activity

Bursts were identified as discrete events consisting of a sequence of spikes with burst onset defined by two consecutive spikes within an interval less than mean interspike interval ($\overline{ISI}$) in a trace with set parameters, and burst termination defined by an ISI greater than $\overline{ISI} + 500\,msec$). Duty cycle ($DC$) was calculated as the burst duration divided by the cycle period (Figure 2B). Spike frequency was calculated as mean frequency of spikes within bursts.

Burst detection based on the slow wave

Traces were low pass filtered to 1 Hz and smoothed using moving average filter with 100 data points windows. Then slow-wave peaks of membrane potential oscillations were detected using local maxima detection algorithm, with a threshold of mean value of filtered membrane potential ($\overline{V_M}$) + 2.5 mV and a peak prominence of 3. Slow-wave dips were detected using the same algorithm for the inverted filtered traces. Slow-wave amplitude of membrane potential oscillation were calculated as the difference between peak and dip values. Cycle frequency of bursting circuits was calculated as an inverse of oscillation period determined by thresholding the filtered traces. Threshold was set to half the amplitude of the slow wave.

We manually inspected the traces to ensure the accuracy of bursts and spikes identification.

Classification of a circuit activity pattern

Similar to Grashow et al. (2009), we classified the activity patterns of reciprocally inhibitory circuits into silent, asymmetric, irregular spiking and antiphase bursting (or half-center oscillations). To refine classification, we also added a 5th category, antiphase spiking (Figure S1 A).

Activity pattern was classified as silent if both neurons fired less than 5 spikes in 1 minute. If only one of the cells fired more than 5 spikes in 1 minute, the activity pattern was classified as asymmetric. If both cells were spiking, the pattern was classified as either irregular spiking, antiphase spiking or bursting. To distinguish these activity patterns, we calculated a measurement of burst exclusion, $\chi_{network}$, described in Grashow et al. (2009). This measure ranges from -1 (simultaneous bursts) to +1 (alternating bursts).

We determined active time intervals for each cell: if the neurons were bursting, the active time intervals were defined as the time from the first to the last spike in the burst, otherwise the active time intervals were defined as ¼ the average interspike interval and centered on each spike. We then calculated the total active time for each cell, t_{cell1} and t_{cell2} as a sum of the active times of each respective cell, and the overlap time (when both cells were active) for the circuit,$O_{network}$. We then compared $O_{network}$

to the overlap times that would be expected for uncorrelated circuits, O_{random}, and the minimum possible overlap time, O_{min}.

$$O_{min} = \begin{cases} T_{trial} - t_{cell1} - t_{cell2} & if\ t_{cell1} + t_{cell2} > T_{trial} \\ 0 & otherwise \end{cases}$$

$$O_{random} = \begin{cases} \min(t_{cell1}, t_{cell2}) - \frac{1}{2}[T_{trial} - max(t_{cell1}, t_{cell2})] & if\ t_{cell1} + t_{cell2} > T_{trial} \\ \frac{\min(t_{cell1}, t_{cell2})^2}{2[T_{trial} - max(t_{cell1}, t_{cell2})]} & otherwise \end{cases}$$

T_{trial} is the total active time of the network, calculated as $T_{trial} = t_{cell1} + t_{cell2} - O_{network}$.

From this we calculated the exclusion factor $\chi_{network}$ as

$$\chi_{network} = \frac{O_{random} - O_{network}}{O_{random} - O_{min}}$$

Circuits with both active cells were categorized as antiphase bursters (or half-center oscillators) if $\chi_{network} \geq 0.1$ and were characterized as spiking otherwise.

Finally, to determine whether the network exhibited antiphase spiking pattern of activity, we calculated percent of single spikes in bursts. If the percent of single spikes in bursts was more than 80%, we characterized the activity pattern of these circuits as antiphase spiking.

Spectral Analysis (Figures 5, 6, S2)

Spectrograms for the temperature experiments were calculated using the Burg (1967) method for estimation of the power spectral density in each time window. The Burg method fits the autoregressive (AR) model of a specified order *p* in the time series by minimizing the sum of squares of the residuals. The fast-Fourier transform (FFT) spectrum is estimated using the previously calculated AR coefficients. This method is characterized by higher resolution in the frequency domain than traditional FFT spectral analysis, especially for a relatively short time window (Buttkus, 2000). We used the following parameters for the spectral estimation: data window of 3.2 s, 50% overlap to calculate the spectrogram, and number of estimated AR coefficients *p* = (window/4) + 1. Before calculating power spectrum, voltage traces were low-pass filtered at 2 Hz using a six-order Butterworth filter and down-sampled.

Statistics

To determine whether the duty cycle and spike frequency significantly increased/decreased with ERQ respectively, we measured the Spearman rank correlation coefficient (ρ) between the mean values of these characteristic and ERQ (Figure 2D). The Spearman correlation coefficient measures the strength and direction of correlation between two variables. $\rho = 1$ indicates that the two variables are a perfect monotone function of each other.

To determine the g_H-g_{Syn} conductances sets that produce statistically similar characteristics of the output of half-centers with escape and release mechanisms we performed Wilcoxon rank-sum test for each set of g_H-g_{Syn} conductances (Figure 3B-F). Significance level was set to 0.05. The conductances sets producing the circuit output characteristics that were not significantly different ($p > 0.05$) are indicated by the red boxes in Figure 3.

To determine whether the GM neurons resting membrane potentials, spike amplitudes and input resistances were significantly different at $10℃$ and $20℃$ we performed paired-sample Wilcoxon signed rank-sum test (Figure 5C,D). The results of the statistical test can be found in the legend of Figure 5.

To determine whether the characteristics of the output of half-centers with different oscillatory mechanisms and Q_{10}s were significantly different between $10℃$ and $20℃$ we performed paired-sample Wilcoxon singed rank-sum test (Figure 6F). Significance level was set to 0.05. The results of the statistical test can be found in Table S2. To determine whether the changes in characteristics with an increase in temperature were significantly different between the circuits with release and escape mechanisms and different temperature-dependences we performed one-way ANOVA with Tuckey post-hoc using IBM SPSS Statistics 24. The results of one-way ANOVA can be found in Tables S3-8.

To determine whether the characteristics of the circuit output were significantly different after the addition of the neuromodulatory current we performed paired-sample t-test (Figure 8D1-5). Significance level was set to 0.05. The results of the statistical test can be found in the legend of Figure 8.

References

Alonso, L.M., and Marder, E. (2020). Temperature compensation in a small rhythmic circuit. Elife *9*, e55470.

Amendola, J., Woodhouse, A., Martin-Eauclaire, M.F., and Goaillard, J.M. (2012). Ca^{2+}/cAMP-sensitive covariation of I_A and I_H voltage dependences tunes rebound firing in dopaminergic neurons. J Neurosci *32*, 2166-2181.

Angstadt, J.D., and Calabrese, R.L. (1989). A hyperpolarization-activated inward current in heart interneurons of the medicinal leech. J Neurosci *9*, 2846-2857.

Angstadt, J.D., and Calabrese, R.L. (1991). Calcium currents and graded synaptic transmission between heart Interneurons of the leech. J Neurosi *11*, 746-759.

Arbas, E.A., and Calabrese, R.L. (1987a). Ionic conductances underlying the activity of interneurons that control heartbeat in the medicinal leech. J Neurosci *7*, 3945-3952.

Arbas, E.A., and Calabrese, R.L. (1987b). Slow oscillations of membrane potential in interneurons that control heartbeat in the medicinal leech. J Neurosci *7*, 3953-3960.

Bartos, M., Manor, Y., Nadim, F., Marder, E., and Nusbaum, M.P. (1999). Coordination of fast and slow rhythmic neuronal circuits. J Neurosci *19*, 6650-6660.

Blitz, D.M., and Nusbaum, M.P. (2011). Neural circuit flexibility in a small sensorimotor system. Curr Opin Neurobiol *21*, 544-552.

Brown, T.G. (1911). The intrinsic factors in the act of progression in the mammal. Proc R Soc Lond Biol *84*, 308-319.

Buchholtz, F., Golowasch, J., Epstein, I.R., and Marder, E. (1992). Mathematical model of an identified stomatogastric ganglion neuron. J Neurophysiol *67*, 332-340.

Burg, J.P. (1967). Maximum entropy spectral analysis. Paper presented at: Proc 37th Meeting Society of Exploration Geophysicist (Oklahoma City, OK).

Buttkus, B. (2000). Spectral Analysis and Filter Theory (Berlin: Springer).

Calabrese, R.L. (1998). Cellular, synaptic, network, and modulatory mechanisms involved in rhythm generation. Curr Opin Neurobiol *8*, 710-717.

Calabrese, R.L., Norris, B.J., and Wenning, A. (2016). The neural control of heartbeat in invertebrates. Curr Opin Neurobiol *41*, 68-77.

Calabrese, R.L., Norris, B.J., Wenning, A., and Wright, T.M. (2011). Coping with variability in small neuronal networks. Integrative and comparative biology *51*, 845-855.

Caplan, J.S., Williams, A.H., and Marder, E. (2014). Many parameter sets in a multicompartment model oscillator are robust to temperature perturbations. J Neurosci *34*, 4963-4975.

Daun, S., Rubin, J.E., and Rybak, I.A. (2009). Control of oscillation periods and phase durations in half-center central pattern generators: a comparative mechanistic analysis. J Comput Neurosci *27*, 3-36.

Doloc-Mihu, A., and Calabrese, R.L. (2014). Identifying crucial parameter correlations maintaining bursting activity. PLoS computational biology *10*, e1003678.

Getting, P.A. (1989). Emerging principles governing the operation of neural networks. Annu Rev Neurosci *12*, 185-204.

Goaillard, J.M., and Marder, E. (2021). Ion Channel Degeneracy, Variability, and Covariation in Neuron and Circuit Resilience. Annu Rev Neurosci.

Goaillard, J.M., Taylor, A.L., Schulz, D.J., and Marder, E. (2009). Functional consequences of animal-to-animal variation in circuit parameters. Nat Neurosci *12*, 1424-1430.

Goldman, M.S., Golowasch, J., Marder, E., and Abbott, L.F. (2001). Global structure, robustness, and modulation of neuronal models. J Neurosci *21*, 5229-5238.

Grashow, R., Brookings, T., and Marder, E. (2009). Reliable neuromodulation from circuits with variable underlying structure. Proc Natl Acad Sci U S A *106*, 11742-11746.

Gutierrez, G.J., and Grashow, R.G. (2009). *Cancer borealis* stomatogastric nervous system dissection. In J Vis Exp.

Haddad, S.A., and Marder, E. (2018). Circuit Robustness to Temperature Perturbation Is Altered by Neuromodulators. Neuron *100*, 609-623.

Hill, A.A., Lu, J., Masino, M.A., Olsen, O.H., and Calabrese, R.L. (2001). A model of a segmental oscillator in the leech heartbeat neuronal network. J Comput Neurosci *10*, 281-302.

Katz, P.S. (2016). Evolution of central pattern generators and rhythmic behaviours. Philos Trans R Soc Lond B Biol Sci *371*, 20150057.

Khorkova, O., and Golowasch, J. (2007). Neuromodulators, not activity, control coordinated expression of ionic currents. J Neurosci *27*, 8709-8718.

Kirby, M.S., and Nusbaum, M.P. (2007). Peptide hormone modulation of a neuronally modulated motor circuit. J Neurophysiol *98*, 3206-3220.

Kushinsky, D., Morozova, E.O., and Marder, E. (2019). In vivo effects of temperature on the heart and pyloric rhythms in the crab *Cancer borealis*. J Exp Biol *222*.

Li, X., Bucher, D., and Nadim, F. (2018). Distinct Co-modulation rules of synapses and voltage-gated currents coordinate interactions of multiple neuromodulators. J Neurosci *38*, 8549-8562.

Marder, E., and Bucher, D. (2007). Understanding circuit dynamics using the stomatogastric nervous system of lobsters and crabs. Annu Rev Physiol *69*, 291-316.

Marder, E., and Calabrese, R.L. (1996). Principles of rhythmic motor pattern generation. Physiol Rev *76*, 687-717.

Marder, E., and Eisen, J.S. (1984). Transmitter identification of pyloric neurons: electrically coupled neurons use different transmitters. J Neurophysiol *51*, 1345-1361.

Marder, E., and Goaillard, J.M. (2006). Variability, compensation and homeostasis in neuron and network function. Nat Rev Neurosci *7*, 563-574.

Nadim, F., Olsen, Ø.H., De Schutter, E., and Calabrese, R.L. (1995). Modeling the leech heartbeat elemental oscillator. I. Interactions of intrinsic and synaptic currents. J Comput Neurosci *2*, 215-235.

O'Leary, T., and Marder, E. (2016). Temperature-robust neural function from activity-dependent ion channel regulation. Current Biology *26*, 2935-2941.

Olypher, A.V., and Calabrese, R.L. (2007). Using constraints on neuronal activity to reveal compensatory changes in neuronal parameters. J Neurophysiol *98*, 3749-3758.

Onasch, S., and Gjorgjieva, J. (2020). Circuit Stability to Perturbations Reveals Hidden Variability in the Balance of Intrinsic and Synaptic Conductances. J Neurosci *40*, 3186-3202.

Patel, Y.A., George, A., Dorval, A.D., White, J.A., Christini, D.J., and Butera, R.J. (2017). Hard real-time closed-loop electrophysiology with the Real-Time eXperiment Interface (RTXI). PLoS Comput Biol *13*, e1005430.

Perkel, D.H., and Mulloney, B. (1974). Motor pattern production in reciprocally inhibitory neurons exhibiting postinhibitory rebound. Science *185*, 181-183.

Powell, D., Haddad, S.A., Gorur-Shandilya, S., and Marder, E. (2021a). Coupling between fast and slow oscillator circuits in *Cancer borealis* is temperature-compensated. Elife *10*, e60454

Powell, D.J., Marder, E., and Nusbaum, M.P. (2021b). Perturbation-specific responses by two neural circuits generating similar activity patterns. Curr Biol *31*, 1-8.

1075 Prinz, A.A., Billimoria, C.P., and Marder, E. (2003). Alternative to hand-tuning conductance-
1076 based models: construction and analysis of databases of model neurons. J
1077 Neurophysiol *90*, 3998-4015.
1078 Prinz, A.A., Bucher, D., and Marder, E. (2004). Similar network activity from disparate circuit
1079 parameters. Nat Neurosci *7*, 1345-1352.
1080 Rinberg, A., Taylor, A.L., and Marder, E. (2013). The effects of temperature on the stability of
1081 a neuronal oscillator. PLoS Comput Biol *9*, e1002857.
1082 Roffman, R.C., Norris, B.J., and Calabrese, R.L. (2012). Animal-to-animal variability of
1083 connection strength in the leech heartbeat central pattern generator. J Neurophysiol
1084 *107*, 1681-1693.
1085 Sakurai, A., and Katz, P.S. (2016). The central pattern generator underlying swimming in
1086 Dendronotus iris: a simple half-center network oscillator with a twist. J Neurophysiol
1087 *116*, 1728-1742.
1088 Satterlie, R.A. (1985). Reciprocal inhibition and postinhibitory rebound produce
1089 reverberation in a locomotor pattern generator. Science *229*, 402-404.
1090 Schulz, D.J., Goaillard, J.M., and Marder, E. (2006). Variable channel expression in identified
1091 single and electrically coupled neurons in different animals. Nat Neurosci *9*, 356 -
1092 362.
1093 Schulz, D.J., Goaillard, J.M., and Marder, E.E. (2007). Quantitative expression profiling of
1094 identified neurons reveals cell-specific constraints on highly variable levels of gene
1095 expression. Proc Natl Acad Sci U S A *104*, 13187-13191.
1096 Sharp, A.A., Skinner, F.K., and Marder, E. (1996). Mechanisms of oscillation in dynamic clamp
1097 constructed two-cell half-center circuits. J Neurophysiol *76*, 867-883.
1098 Skinner, F.K., Kopell, N., and Marder, E. (1994). Mechanisms for oscillation and frequency
1099 control in reciprocal inhibitory model neural networks. J Comput Neurosci *1*, 69-87.
1100 Soffe, S.R., Zhao, F.Y., and Roberts, A. (2001). Functional projection distances of spinal
1101 interneurons mediating reciprocal inhibition during swimming in Xenopus tadpoles.
1102 Eur J Neurosci *13*, 617-627.
1103 Soofi, W., Goeritz, M.L., Kispersky, T.J., Prinz, A.A., Marder, E., and Stein, W. (2014). Phase
1104 maintenance in a rhythmic motor pattern during temperature changes *in vivo*. J
1105 Neurophysiol *111*, 2603-2613.
1106 Soofi, W., and Prinz, A.A. (2015). Differential effects of conductances on the phase resetting
1107 curve of a bursting neuronal oscillator. Journal of Computational Neuroscience *38*,
1108 539-558.
1109 Srikanth, S., and Narayanan, R. (2015). Variability in State-Dependent Plasticity of Intrinsic
1110 Properties during Cell-Autonomous Self-Regulation of Calcium Homeostasis in
1111 Hippocampal Model Neurons. eNeuro *2*.
1112 Städele, C., Heigele, S., and Stein, W. (2015). Neuromodulation to the rescue: compensation
1113 of temperature-induced breakdown of rhythmic motor patterns via extrinsic
1114 neuromodulatory input. PLoS Biol *13*, e1002265.
1115 Swensen, A.M., and Bean, B.P. (2005). Robustness of burst firing in dissociated purkinje
1116 neurons with acute or long-term reductions in sodium conductance. J Neurosci *25*,
1117 3509-3520.
1118 Swensen, A.M., and Marder, E. (2000). Multiple peptides converge to activate the same
1119 voltage-dependent current in a central pattern-generating circuit. J Neurosci *20*,
1120 6752-6759.
1121 Swensen, A.M., and Marder, E. (2001). Modulators with convergent cellular actions elicit
1122 distinct circuit outputs. J Neurosci *21*, 4050-4058.

Tang, L.S., Goeritz, M.L., Caplan, J.S., Taylor, A.L., Fisek, M., and Marder, E. (2010). Precise temperature compensation of phase in a rhythmic motor pattern. PLoS Biol *8*, e1000469.

Tang, L.S., Taylor, A.L., Rinberg, A., and Marder, E. (2012). Robustness of a rhythmic circuit to short- and long-term temperature changes. J Neurosci *32*, 10075-10085.

Temporal, S., Desai, M., Khorkova, O., Varghese, G., Dai, A., Schulz, D.J., and Golowasch, J. (2012). Neuromodulation independently determines correlated channel expression and conductance levels in motor neurons of the stomatogastric ganglion. J Neurophysiol *107*, 718-727.

Tobin, A.E., Cruz-Bermudez, N.D., Marder, E., and Schulz, D.J. (2009). Correlations in ion channel mRNA in rhythmically active neurons. PLoS ONE *4*, e6742.

Tran, T., Unal, C.T., Severin, D., Zaborszky, L., Rotstein, H.G., Kirkwood, A., and Golowasch, J. (2019). Ionic current correlations are ubiquitous across phyla. Sci Rep *9*, 1687.

Wang, X.-J., and Rinzel, J. (1992). Alternating and synchronous rhythms in reciprocally inhibitory model neurons. Neural Comp *4*, 84-97.

Xu, H., and Robertson, M.R. (1994). Effects of temperature on properties of flight neurons in the locust. J Comp Physiol [A] *174*, 193-202.

Xu, H., and Robertson, R.M. (1996). Neural parameters contributing to temperature compensation in the flight CPG of the locust, *Locusta migratoria*. Brain Res *734*, 213-222.

Zang, Y., Hong, S., and De Schutter, E. (2020). Firing rate-dependent phase responses of Purkinje cells support transient oscillations. eLife *9*.

Zhang, C., and Lewis, T.J. (2013). Phase response properties of half-center oscillators. J Comput Neurosci *35*, 55-74.

Zhao, S., and Golowasch, J. (2012). Ionic current correlations underlie the global tuning of large numbers of neuronal activity attributes. J Neurosci *32*, 13380-13388.

Supplementary Tables. Summary statistics for figure 7.

Table S1

	Escape						Release					
	10°C			20°C			10°C			20°C		
	$Q_{10}=1$	$Q_{10}=2$ for g_H, g_{Syn}	$Q_{10}=2$	$Q_{10}=1$	$Q_{10}=2$ for g_H, g_{Syn}	$Q_{10}=2$	$Q_{10}=1$	$Q_{10}=2$ for g_H, g_{Syn}	$Q_{10}=2$	$Q_{10}=1$	$Q_{10}=2$ for g_H, g_{Syn}	$Q_{10}=2$
Cycle freq, Hz	0.23 ± 0.07	0.20 ± 0.09	0.20 ± 0.07	0.23 ± 0.08	0.20 ± 0.09	0.46 ± 0.19	0.19 ± 0.05	0.23 ± 0.09	0.26 ± 0.11	0.28 ± 0.09	0.14 ± 0.06	0.30 ± 0.11
Spike freq, Hz	7.9 ± 2.9	6.6 ± 2.1	6.7 ± 1.1	10.1 ± 4.8	13.7 ± 4.3	19.4 ± 2.0	7.7 ± 4.1	5.9 ± 2.8	7.9 ± 1.8	9.1 ± 4.6	10.4 ± 3.7	15.7 ± 3.1
Amplitude, mV	22.7 ± 6.3	21.6 ± 1.0	21.8 ± 2.4	21.5 ± 6.2	27.5 ± 4.4	23.8 ± 4.4	27.9 ± 4.8	20.0 ± 7.3	19.6 ± 5.3	20.6 ± 4.3	32.7 ± 10.3	30.3 ± 10.3
# spikes/burst	9 ± 5	7 ± 1	7 ± 2	13 ± 8	18 ± 5	9 ± 4	18 ± 13	12 ± 9	14 ± 6	15 ± 11	36 ± 23	25 ± 7
Duty cycle, %	25.8 ± 9.9	20.1 ± 5.2	17.4 ± 0.4	26.7 ± 10.2	24.6 ± 5.5	17.0 ± 1.6	42.0 ± 4.6	36.2 ± 10.6	41.7 ± 4.4	40.0 ± 5.3	39.5 ± 6.2	44.8 ± 2.9
ERQ	-0.08 ± 0.03	-0.07 ± 0.02	-0.08 ± 0.02	-0.07 ± 0.03	-0.09 ± 0.03	-0.10 ± 0.02	0.13 ± 0.05	0.15 ± 0.07	0.14 ± 0.07	0.14 ± 0.05	0.15 ± 0.07	0.14 ± 0.08

Table S2

Paired-samples Wilcoxon signed rank test for cycle frequency at 10°C vs 20°C

Mechanism	Q_{10}	N	p-value
Escape	1	11	.100
	2 for g_H, g_{Syn}	4	.144
	2	3	.109
Release	1	6	**.028**
	2 for g_H, g_{Syn}	5	**.043**
	2	4	.144

Paired-samples Wilcoxon signed rank test for spike frequency at 10°C vs 20°C

Mechanism	Q_{10}	N	p-value
Escape	1	21	**<.001**
	2 for g_H, g_{Syn}	8	**.012**
	2	6	**.028**
Release	1	12	**.003**
	2 for g_H, g_{Syn}	10	**.005**
	2	8	**.012**

Paired-samples Wilcoxon signed rank test for # spikes/burst at 10°C vs 20°C

Mechanism	Q_{10}	N	p-value
Escape	1	21	**<.001**
	2 for g_H, g_{Syn}	8	**0.018**
	2	6	.246
Release	1	12	**.041**
	2 for g_H, g_{Syn}	10	**.005**
	2	8	**.018**

Paired-samples Wilcoxon signed rank test for amplitude at 10°C vs 20°C

Mechanism	Q_{10}	N	p-value
Escape	1	21	**.011**
	2 for g_H, g_{Syn}	8	**.012**
	2	6	.075
Release	1	12	**.002**
	2 for g_H, g_{Syn}	10	**.005**
	2	8	**.012**

Paired-samples Wilcoxon signed rank test for duty cycle at 10°C vs 20°C

Mechanism	Q_{10}	N	p-value
Escape	1	21	.590
	2 for g_H, g_{Syn}	8	.123
	2	6	.753
Release	1	12	.388
	2 for g_H, g_{Syn}	10	.646
	2	8	**.036**

Paired-samples Wilcoxon signed rank test for ERQ at 10°C vs 20°C

Mechanism	Q_{10}	N	p-value
Escape	1	21	**.009**
	2 for g_H, g_{Syn}	8	**.017**
	2	6	.173
Release	1	12	.136
	2 for g_H, g_{Syn}	10	.286
	2	8	.575

Table S3

Measure: change in cycle frequency from 10°C to 20°C; Test: One-way ANOVA; F-statistic: F(5,59)=21.790, p<0.001; Post-hoc: Tuckey							
		Escape			Release		
	Q_{10}	1 *all*	2 *for* g_s, g_{Syn}	2 *all*	1 *all*	2 *for* g_s, g_{Syn}	2 *all*
Escape	1 *all*		.999	**<.001**	**.014**	**.053**	.540
	2 for g_H, g_{Syn}			**<.001**	.147	.101	.864
	2 *all*				**<.001**	**<.001**	**<.001**
Release	1 *all*					**<.001**	.781
	2 for g_H, g_{Syn}						**.006**
	2 *all*						

Table S4

Measure: change in spike frequency from 10°C to 20°C; Test: One-way ANOVA; F-statistic: F(5,59)=9.897, p<0.001; Post-hoc: Tuckey							
		Escape			Release		
	Q_{10}	1 *all*	2 *for* g_s, g_{Syn}	2 *all*	1 *all*	2 *for* g_s, g_{Syn}	2 *all*
Escape	1 *all*		**.023**	**<.001**	.981	.580	**.006**
	2 for g_H, g_{Syn}			.276	**.011**	.660	.999
	2 *all*				**<.001**	**.007**	.483
Release	1 *all*					.324	**.003**
	2 for g_H, g_{Syn}						.397
	2 *all*						

Table S5

Measure: change in # spikes/burst from 10°C to 20°C; Test: One-way ANOVA; F-statistic: F(5,59)=13.949, p<0.001; Post-hoc: Tuckey							
		Escape			Release		
	Q_{10}	1 *all*	2 *for* g_s, g_{Syn}	2 *all*	1 *all*	2 *for* g_s, g_{Syn}	2 *all*
Escape	1 *all*		.229	.999	.286	**<.001**	.279
	2 for g_H, g_{Syn}			.354	**.005**	**.020**	1.00
	2 *all*				.818	**<.001**	.391
Release	1 *all*					**<.001**	**.007**
	2 for g_H, g_{Syn}						**.015**
	2 *all*						

Table S6

Measure: change in amplitude from 10°C to 20°C; Test: One-way ANOVA; F-statistic: F(5,59)=50.437, p<0.001; Post-hoc: Tuckey							
		Escape			Release		
	Q_{10}	1 *all*	2 *for* g_s, g_{Syn}	2 *all*	1 *all*	2 *for* g_s, g_{Syn}	2 *all*
Escape	1 *all*		**<.001**	.406	**<.001**	**<.001**	**<.001**
	2 for g_H, g_{Syn}			.314	**<.001**	**.002**	.082
	2 *all*				**<.001**	**<.001**	**<.001**
Release	1 *all*					**<.001**	**<.001**
	2 for g_H, g_{Syn}						.853
	2 *all*						

Table S7

Measure: change in duty cycle from 10°C to 20°C; Test: One-way ANOVA; F-statistic: F(5,59)= 0.964, p=0.447; Post-hoc: Tuckey							
		Escape			Release		
	Q_{10}	1 *all*	2 *for* g_s, g_{Syn}	2 *all*	1 *all*	2 *for* g_s, g_{Syn}	2 *all*
Escape	1 *all*		.821	1.00	.961	.939	.964
	2 for g_H, g_{Syn}			.865	.489	.999	.999
	2 *all*				.999	.948	.964
Release	1 *all*					.647	.729
	2 for g_H, g_{Syn}						.000
	2 *all*						

Table S8

Measure: change in ERQ from 10°C to 20°C; Test: One-way ANOVA; F-statistic: F(5,59)=4.076, p=0.003; Post-hoc: Tuckey							
		Escape			Release		
	Q_{10}	1 *all*	2 *for* g_s, g_{Syn}	2 *all*	1 *all*	2 *for* g_s, g_{Syn}	2 *all*
Escape	1 *all*		**.019**	**.033**	.970	1.00	.549
	2 for g_H, g_{Syn}			1.00	.177	**.040**	.757
	2 *all*				.208	**.054**	.747
Release	1 *all*					.963	.942
	2 for g_H, g_{Syn}						.592
	2 *all*						